Nanostructured Materials for Photolytic Hydrogen Production

Jiefang Zhu, Dinko Chakarov and Michael Zäch

Abstract A hydrogen economy is often considered an attractive alternative to our current fossil fuel-based energy system. In order for such a hydrogen economy to become reality, several challenges associated with the production, storage, transportation and use of hydrogen must be solved. This chapter addresses the issue of hydrogen production. While the currently most widely used method to produce hydrogen is based on the conversion of fossil fuel resources and does not therefore fulfill the requirement of CO_2 neutrality, we discuss here the photolytic production of hydrogen via water splitting. This scheme is based on energy input from the most powerful and ultimately sustainable energy source mankind has at its disposal: the sun. Moreover, no carbon dioxide is released into the atmosphere, and the method has potential for cost-effective large-scale production.

1 Background and Introduction

Mankind is facing two challenges of hitherto unsurpassed importance and complexity, namely the "tera-Watt" and "tera-ton" challenges. The former refers to the issue of supplying a rapidly growing world population with larger and larger

J. Zhu (✉)
Department of Materials Chemistry, Uppsala University,
Lägerhyddsvägen 1,
751 21 Uppsala, Sweden
e-mail: jiefang.zhu@mkem.uu.se

D. Chakarov · M. Zäch
Department of Applied Physics, Chalmers University of Technology,
Fysikgränd 3, 412 96 Göteborg, Sweden
e-mail: michael.zach@chalmers.se

amounts of energy [1], while the latter encompasses finding ways to deal with the huge amounts of carbon dioxide being emitted into the atmosphere as a consequence of our fossil fuel-based energy system [2]. The formidable task is to identify an alternative energy system, which at the same time is sustainable, virtually unlimited, safe and clean. The task becomes yet more challenging when also considering economy and security of supply aspects.
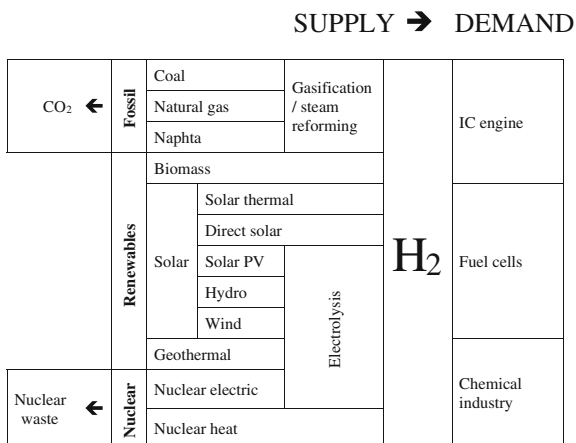
The hydrogen economy is one of many suggested scenarios that may be able to address these tera-challenges. The basic idea of the hydrogen economy is that hydrogen—a light, diatomic gas with a vast energy content by weight, but a small energy content per volume—would replace the fossil fuels which form the backbone of our current energy system. Hydrogen reacts cleanly with oxygen in a highly exothermic reaction, with pure water being the only exhaust product. The energy stored in the chemical bond of hydrogen can thus be released by burning it in a combustion engine, or more efficiently by oxidizing it in a fuel cell. Apart from zero-emissions, hydrogen has further attractive properties, including that it can be stored and transported, which are crucial requirements addressing the typically intermittent nature of renewable energy sources. In order for hydrogen to become an economically viable option, several hurdles must be surpassed. Besides providing efficient, inexpensive and durable fuel cells, the production of hydrogen and its storage constitute two other important cornerstones of the hydrogen economy. The former aspect will be discussed in this chapter, while the latter is covered separately in different chapters of this book.

1.1 Overview of Current and Potential Future Hydrogen Production Methods

While hydrogen (H) is abundant on earth, molecular hydrogen (H_2) is usually not found in large quantities in nature. Most of the hydrogen is bound to carbon, oxygen or both, meaning that H_2 must be generated by extracting it from other hydrogen sources via highly endothermic processes. The energy required to drive these extraction processes may come from essentially any energy source, including renewable energy sources, as illustrated in Fig. 1. A key aspect to bear in mind is that hydrogen is not an energy source but an energy vector.

A large fraction of today's hydrogen production is based on fossil fuel resources. The processes involved in the conversion of fossil fuels, such as the reforming of natural gas, coal gasification/liquefaction and coal electrolysis, require large amounts of energy, either in the form of heat or electricity, and all these methods are associated with the release of vast amounts of carbon dioxide. For the hydrogen economy to become a viable option of our energy future, we therefore have to access other feedstocks from which hydrogen can be produced, and we have to make sure that the energy required to transform these feedstocks to hydrogen is provided by a sustainable and carbon–neutral source. Alternative feedstocks under consideration include wood, other biomass, organic waste and

Fig. 1 Schematic illustration of various hydrogen production pathways using different primary energy sources and energy conversion schemes. The main application areas of hydrogen and unwanted emissions from selected processes are indicated on the right and left hand side, respectively

SUPPLY ➜ DEMAND

CO_2 ←	Fossil	Coal	Gasification / steam reforming		IC engine
		Natural gas			
		Naphta			
	Renewables	Biomass			
		Solar thermal			
		Direct solar			
		Solar — Solar PV		H_2	Fuel cells
		Hydro	Electrolysis		
		Wind			
		Geothermal			
Nuclear waste ←	Nuclear	Nuclear electric			Chemical industry
		Nuclear heat			

water, where the first three options are not truly carbon neutral. The last option constitutes an entirely sustainable energy system, where hydrogen is produced from water and later on recovered back into water upon conversion in a combustion engine or a fuel cell. This chapter therefore focuses on hydrogen production from water. In principle, water can be split into hydrogen and oxygen along several different pathways and utilizing various (sustainable) energy sources. The method used most commonly today is to dissociate water in an electrolysis cell, where the required electricity may be produced from nuclear, geothermal, gravitational or solar energy.[1] Solar energy is clean, quiet, sustainable, and its potential is enormous. The solar influx, i.e., the energy received by the planet from the sun (174 petawatts $= 1.7 \times 10^{17}$W), surpasses the current world energy consumption rate (ca. 15 TW $= 1.5 \times 10^{13}$W) by more than four orders of magnitude. In other words, less than one hour of sunshine would, in principle, be sufficient to provide us with energy for an entire year. Given this enormous potential, various forms of solar energy, including exploiting solar energy for heating and cooling purposes, converting solar energy into electricity using photovoltaic materials or solar thermal technologies and converting solar energy into storable chemical fuels, as discussed in this chapter, have recently received considerable attention.

Since electrolysis is a two-step process, the potential of achieving a highly efficient, simple, and at the same time cost-effective conversion is limited. A more appealing idea is to directly split water into its component gases using a single device without the prior production of electricity, i.e., with no external electron flow. High-temperature thermochemical cycles, i.e., a set of coupled, thermally-driven chemical reactions that sum to the decomposition of water into H_2 and O_2,

---

[1] Note that wind power and hydropower are considered variations of solar energy here, and that solar energy, and to a large extent also geothermal energy, actually are based on nuclear processes.

and photolysis (the direct splitting of water using light as the only energy input), represent two approaches in this direction. The primary heat sources, which are discussed in the context of high-temperature thermochemical cycles, are nuclear energy and solar energy. While thermochemical cycles potentially can be run at high efficiency, they currently either require very high temperatures ($> 1500°C$), where material challenges are significant, or they involve aggressive chemicals. Photolysis-based approaches, on the other hand, can run at ambient temperature because the splitting of water is not thermally induced but achieved via electron–hole pair driven redox reactions. To this end, energy-rich photons from the solar spectrum are harvested in a semiconductor material, where they may excite electron–hole pairs, which in turn may drive chemical reactions at the semiconductor surface.

The latter scheme is the subject of this chapter, which provides an overview of the CO_2-free production of hydrogen via photon-driven redox reactions on semiconductor materials and employing entirely renewable and abundant raw materials and energy sources, namely water and sunlight. Particular attention will be paid to the role of nanoscience and nanotechnology, which have attracted a continuously growing interest in this context, and which have shown a strong potential to improve the efficiency of various hydrogen production methods, not the least approaches based on photolysis.

Before diving into the details, we would like to note that the idea of using water as a raw material for energy production is not an entirely new concept. In 1874, Jules Verne, in his novel *The Mysterious Island*, painted a scenario where *water one day will be employed as fuel*, thereby replacing dwindling coal reserves and driving the machinery without which *there would be no railways, no steamers, no manufactories, nothing of that which is indispensable to modern civilization*. Today, almost 140 years later, Jules Verne's visionary ideas have neither been realized nor abandoned. In fact, the concept of a hydrogen economy still attracts a lot of interest, although the hurdles on the way sometimes seem insurmountable. The hope is that this chapter may provide the reader with an understanding of the state-of-the-art in the field of photolytic hydrogen production and identify the most burning scientific and technological issues that have prevented hydrogen from becoming our prime energy carrier.

The remainder of this chapter is organized as follows: after a general introduction, we briefly review the mechanism and challenges associated with photolytic water-splitting (Sect. 2). In Sect. 3, we present an overview of various semiconductor materials, which have been scrutinized for their ability to split water into hydrogen and oxygen under sunlight illumination. The advantages and shortcomings of these materials will be described. Next, we discuss various ways in which nanoscience and nanotechnology (N&N) can improve materials and their integration into water splitting devices (Sect. 4). Our emphasis is on N&N approaches: (i) to tune the optical and electronic properties of semiconductors, (ii) to manage and optimally utilize the incoming light, (iii) to improve the separation and extraction of photogenerated charge carriers via control of the photocatalyst structure and morphology, (iv) to tailor the transport of reactants and products, and

(v) to fabricate well-defined model systems. We conclude by outlining possible pathways toward sustainable hydrogen production schemes, which challenges need to be addressed on the way, and how N&N may contribute.

2 Mechanism of Photolytic Hydrogen Production

Photolytic water-splitting schemes integrate solar energy collection and water electrolysis into a single device, thereby transforming solar energy into chemical energy in the form of hydrogen. Several steps are required to achieve this transformation, which is initiated by the harvesting of solar photons (see Fig. 2). Since water is essentially transparent to the wavelengths constituting the solar spectrum, photolytic splitting of water requires the presence of a light harvesting structure, typically in the form of a semiconductor. Owing to their particular electronic band structure, semiconductors are able to interact with photons whose energy exceeds a threshold corresponding to the bandgap energy of the material, i.e., the energy separation between the valence and conduction band edges. If this condition is met, an electron may be promoted from the valence band to the conduction band, thereby leaving an empty state, normally referred to as a hole, behind. In order for such an excited electron–hole pair to drive water-splitting, it must have an energy that exceeds the standard potential, ΔE^o, for the decomposition of liquid water to form gaseous hydrogen and oxygen (-1.23 V, where the negative sign indicates that the water-splitting process is thermodynamically non-spontaneous). The excited electron–hole pairs are short lived, and the photogeneration of charge carriers must therefore be followed by efficient charge separation schemes in order for a significant fraction (defined by the quantum yield) of these electron–hole pairs to escape recombination and make their way to the semiconductor surface. If the photogenerated electrons and holes have sufficient energy to reduce protons and to oxidize water, respectively, they may be extracted at the solid/liquid interface and drive the photosplitting of water. Finally, hydrogen and oxygen gas need to be removed from solution and separated from one another in the case of photocatalytic water splitting.

Note that we distinguish here photocatalytic and photoelectrochemical water splitting. In the former case, the reaction takes place in a suspension or colloidal solution of semiconductor nanoparticles. Oxidation and reduction reactions occur in close proximity to one another, and a mixture of hydrogen and oxygen is thus evolved. In the latter case, the semiconductor is made into a photoanode, from which oxygen is evolved. Photogenerated electrons are extracted from the semiconductor by a charge collection layer and, through an external circuit, shuttled to a counter-electrode, where they recombine with protons to form hydrogen. Oxygen and hydrogen production sites are thus spatially separated.

There are several potential bottlenecks, which may hamper or even prevent photolytic water splitting. The most burning issues are summarized as follows: (i) mismatch between the semiconductor's absorption characteristics and the solar
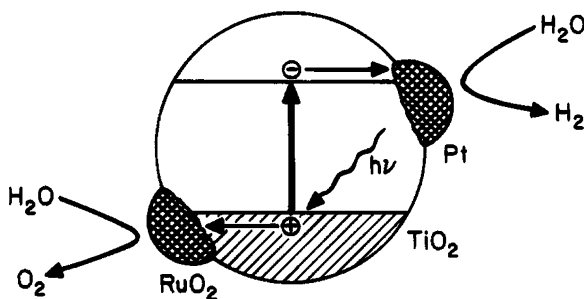
Fig. 2 Schematic illustration of the elementary reaction steps of photocatalytic hydrogen production via water splitting on semiconductor nanoparticles with additional co-catalysts for oxygen and hydrogen evolution. Reprinted with permission from [3]. Copyright 1995 American Chemical Society

spectrum (and other light sources), (ii) inappropriate semiconductor bandgap and/ or band edge positions, (iii) fast (bulk and/or surface) electron–hole recombination, (iv) short lifetime and thus limited diffusion length of photogenerated electrons and/or holes, (v) poor electron and/or hole transfer kinetics at the semiconductor-liquid interface (large over-potentials required), (vi) competing reactions, including photocorrosion and the back-reaction of hydrogen and oxygen to water in the case of photocatalytic water splitting

In the next section, different classes of materials and their properties will be discussed in light of these requirements and issues, followed by Sect. 4, which presents various nanoscience- and nanotechnology-based approaches towards improved photolytic water splitting.

3 Materials for Photolysis of Water

Materials play a key role in photolytic H_2 production, and their structure and electronic properties largely determine the efficiency of each step in the photolysis of water. The majority of photocatalysts and photoanodes are composed of metal oxides (Sects. 3.1–3.3), metal sulfides (Sect. 3.4), metal nitrides (Sect. 3.5), oxysulfides (Sect. 3.6), oxynitrides (Sect. 3.6) and composites thereof (Sect. 3.7). In these cases, metal cations with the highest oxidative states have d^0 (red area in Fig. 3) or d^{10} (green area) electronic configuration, while O, S and N (blue area) show their most negative states. The bottom of the conduction band consists of the d and sp orbitals of the metal cations, while the top of the valence band in metal oxides is composed of O 2p orbitals, which are normally located at ca. +3 V (vs NHE) or higher [4, 5]. The valence bands of metal oxysulfides and oxynitrides are formed by S 3p (and O 2p) and N 2p (and O 2p), respectively. Some alkali (Li, Na, K, Rb and Cs), alkaline earth (Mg, Ca, Sr and Ba) and transition metal

Fig. 3 Elements constructing photocatalysts for water splitting

(Y, La and Gd) ions can construct a crystal structure of layered perovskite and cubic pyrochlore compounds, but do not contribute to the energy band structure of these compounds [5]. In this section, the most widely used materials for photolytic H_2 production will be introduced. The focus is on material properties, which influence the photoconversion efficiency.

3.1 Titanium Dioxide (TiO₂)

Compared to other photoactive materials for H_2 production, TiO_2 has received much attention since the initial work of Fujishima and Honda [6] due to its low cost, abundance, stability and performance.

Despite a high rate of consumption, a shortage of TiO_2 seems impossible in the near future. Titanium is the ninth most abundant element in the world and constitutes about 0.63% in weight of the Earth's crust. Minerals, like rutile (TiO_2) and ilmenite ($FeTiO_3$), are the main ores of this element, and they are found in large deposits in Norway, Australia, China, Canada and many other countries [7]. The toxicity of TiO_2 is low, and it has been approved as a food colorant (E-171 in EU legislation). Actually, TiO_2 is widely used in many daily products such as toothpaste, pill coatings and chewing gum [8].

TiO_2 has four main crystal phases: anatase (tetragonal), rutile (tetragonal), brookite (orthorhombic) and TiO_2 (B) (monoclinic). All TiO_2 forms can be described as different arrangements of elongated TiO_6 octahedra connected by

sharing corners and edges. These differences in lattice structure determine different mass densities and electronic band structures between different forms of TiO_2. Loose zigzag chains in octahedra coordination exist in anatase and TiO_2 (B) structures, compared to linear chains of octahedra in rutile. Therefore, the interstitial spaces between octahedra in TiO_2 (B) and anatase are larger, making them less compact than rutile and brookite (densities of TiO_2 (B) and anatase are 3.64 and 3.84 g cm^{-3}, respectively, compared to 4.26 g cm^{-3} for rutile and 4.17 g cm^{-3} for brookite) [9, 10]. Compared to anatase and rutile, brookite and TiO_2 (B) are uncommon, unstable and not easily synthesized in their pure phases. Therefore, they are seldom used as independent photocatalysts or photoanodes. Although rutile is the most stable crystal phase of TiO_2, the difference in Gibbs free energies of formation for rutile and anatase is small (less than 15 kJ mol^{-1}) [11]. Generally speaking, anatase will transform to rutile at high temperature, big size and/or small surface area. However, the critical values of this transformation depend on the pH conditions, adsorbates, pressure and preparation methods, which explains some of the conflicts in the literature. It has been shown that bicrystalline TiO_2 (mixture of anatase–rutile, anatase-brookite or anatase-TiO_2 (B)) normally has better photocatalytic and photoelectrochemical performance than its single-phase constituents. This synergistic effect is attributed to the formation of n–p junctions at the contact of the two crystal phases, which improves the efficiency of charge separation.

Due to the presence of a small amount of oxygen vacancies, which are compensated by the presence of Ti^{3+} centers, pure TiO_2 is an *n*-type semiconductor and is transparent to visible light. The top of the TiO_2 valence band is mainly formed by overlapping oxygen 2p orbitals (O $p\pi$ states), whereas the lower part of its conduction band is mainly constituted by the 3d orbitals (t_{2g} bands) of Ti^{4+} cations [12]. The band gaps are 3.2 eV (corresponding to an absorption edge of 380 nm) and 3.0 eV (400 nm) for anatase and rutile, respectively, which limits their ability to convert visible light. Another drawback of TiO_2 is its low photon efficiency. The band transitions of TiO_2 are indirect, and indirect-band semiconductors normally present less photon absorption compared to direct-band semiconductors. In addition, 90% of the photogenerated electron–hole pairs have short lifetimes and recombine in less than 10 ns; the photogenerated carriers available for surface reactions are very limited. Quantum yields for TiO_2 reactions in solution are typically below 1%, while they can exceed 25% for some gas-phase reactions. The values depend largely on the electronic transport at different interfaces and surfaces [13].

The conduction band energy E_{CB} of rutile coincides with the reversible hydrogen potential ($E^{H^+/H_2} = 0 V vs. NHE at pH 0$), whereas that for anatase is more negative by 0.2 eV. The valence band energy E_{VB} of both anatase and rutile is more than positive enough to oxidize water ($E_{O_2/H_2O} = 1.2$ V vs. NHE at pH 0), by about 1.8 eV. Note that these relationships are relatively fixed, since both E_{CB}, E_{VB}, and reduction and oxidation potentials simultaneously shift with solution pH (–59 mV per pH unit). Therefore, one of the main advantages of TiO_2 over other

semiconductors is that its electronic structure allows both the reduction of protons and the oxidation of water, which are key processes for water splitting. TiO_2 is photo-corrosion resistant because water oxidation is thermodynamically more favored than the oxidation of oxide anions by photogenerated holes. This stability, which is maintained over a large pH range, is a crucial feature and explains the widespread use of TiO_2 in water splitting [13].

3.2 Other Binary Metal Oxides

In addition to TiO_2, there are some other traditional metal oxides, which have also been investigated extensively due to their specific advantages. Among them, ZnO, α-Fe_2O_3 and WO_3 are representative. However, they all have inherent drawbacks in photolytic H_2 production.

ZnO has a large application potential in optoelectronic devices, due to its diverse physical properties and finely tunable preparation. ZnO normally has a hexagonal (wurtzite) structure with the lattice parameters a = b = 3.25 Å and c = 5.12 Å. ZnO is intrinsically doped via oxygen and/or zinc interstitials, which act as *n*-type donors. However, it can be designed and doped to be either *n*- or *p*-type. ZnO is a direct-band gap semiconductor, and has a wide band gap of 3.2 eV with good charge carrier mobility. ZnO has similar conduction and valence positions as anatase TiO_2, as shown in Fig. 4, and therefore has been frequently considered an alternative to TiO_2 for photocatalytic applications. Although ZnO and TiO_2 have similar conduction band positions, the density of states is about one order of magnitude lower in ZnO. Also, the structure of the conduction bands differs. The conduction band of ZnO is mainly composed of Zn 4s and 4p orbitals, while that of TiO_2 consists of Ti 3d orbitals [14]. This may affect the transfer rate of photogenerated electrons from the valence band to the conduction band under irradiation. The electron mobility in single-crystalline ZnO is much higher than that of anatase TiO_2. It tends to decrease with doping due to electron scattering at impurities, and decreases substantially due to scattering and energy barriers at grain boundaries [14, 15].

The main drawback of ZnO in solution is its chemical instability. It is soluble in strong acids (Eq. 1) and its surface converts to $Zn(OH)_2$ in alkalis (Eq. 2), which limits its application at extreme pH settings as well as in the presence of Zn^{2+} chelating agents.

$$ZnO + 2H^+_{(aq)} \rightarrow Zn^{2+}_{(aq)} + H_2O \qquad (1)$$

$$ZnO + H_2O \rightarrow Zn(OH)_2 \qquad (2)$$
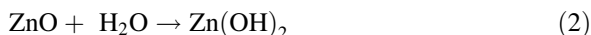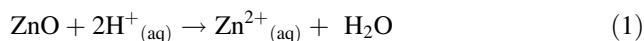
Besides its chemical instability, ZnO is easily photo-corroded, especially at low pH values. Under irradiation for a long time, ZnO suffers from photodecomposition due to the oxidation of O^{2-} in ZnO by photogenerated holes (Eq. 3).
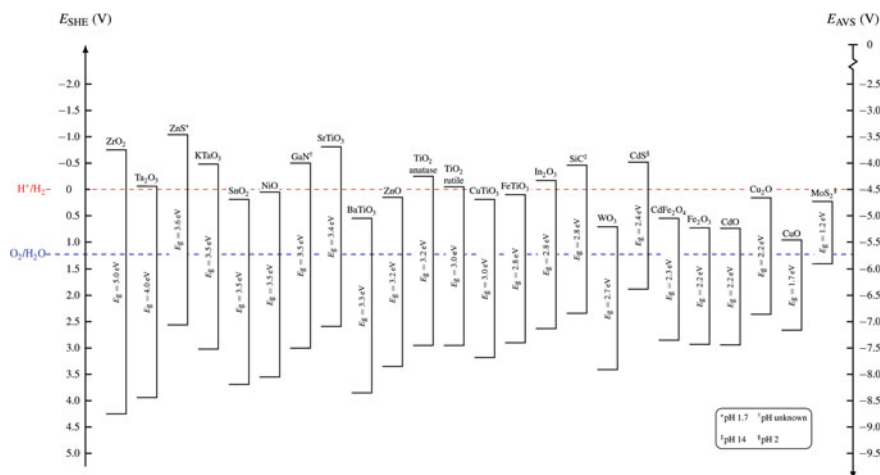
Fig. 4 Valence and conduction band positions of various semiconductors with respect to the standard hydrogen electrode (SHE) and the vacuum reference energy level E_{AVS}. All values are tested at pH 1, unless otherwise noted

$$2ZnO + 4h_{VB}^{+} \rightarrow 2Zn^{2+}{}_{(aq)} + O_{2(g)} \quad (3)$$
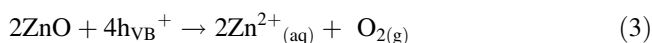
WO_3 is an *n*-type semiconductor with a relatively narrow band gap of 2.7 eV, which enables it to convert part of the visible solar light. Using WO_3 for solar energy conversion has been extensively investigated. WO_3, like TiO_2, is photo-corrosion resistant. The VB of WO_3 is close to that of TiO_2, exceeding the O_2/H_2O potential, which makes it a successful photocatalyst for O_2 evolution from water. However, the bottom of its CB lies below the redox potential of H^+/H_2, which means that the reduction of water to hydrogen is thermodynamically unfavorable for WO_3. Applying a bias can overcome the energy barrier for the ejection of photogenerated electrons from the conduction band to water. Coupling with other semiconductors (like TiO_2) and doping are alternative ways to achieve overall water splitting with WO_3 [16].

α-Fe_2O_3 is another attractive candidate for water splitting due to its narrow band gap (2.2 eV), good photo stability, chemical inertness and the abundance of iron mineral resources in the world. The band structure of α-Fe_2O_3 is similar to that of WO_3, with the VB top more negative, but still exceeding the O_2/H_2O potential, and the CB bottom lower than the redox potential of H^+/H_2. A variety of dopants have been employed to modify α-Fe_2O_3 and *p*-type semiconductor behavior has been obtained, in addition to its common *n*-type characteristics. The main bottlenecks of α-Fe_2O_3 are its fast e^--h^+ recombination rate, poor charge transport characteristics due to the trapping of electrons at defect sites and the poor mobility of holes. Attempts to circumvent these problems by using a bias, scavengers, coupling to

other semiconductors, structure configurations and compositional tuning will contribute to further applications of this material.

There are many other binary metal oxides that have been used in photoelectrolysis of water, such as SnO_2, CeO_2, NiO, CdO, PdO, V_2O_5, MoO_3, Cr_2O_3, In_2O_3, Ga_2O_3, Cu_2O, CuO, Bi_2O_3, ZrO_2, Ta_2O_5 and so on. Although all of them have inherent issues, some of them are very good coupling partners to be used in conjunction with another semiconductor.

3.3 Ternary and Quaternary Metal Oxides

When TiO_2 is fused with other metal oxides (SrO, BaO, Ln_2O_3 (Ln = lanthanide)), metal titanates with the perovskite structure are formed. Perovskites have the general formula, ABX_3, with $SrTiO_3$ as an example. Their framework structure contains corner-sharing TiO_6 octahedral with the A cation in twelve-coordinate interstices. Several hundred oxides own this structure. In addition to the cubic structure exhibited by $SrTiO_3$, a series of distorted, non-cubic structures occurs, with the framework of TiO_6 octahedra being twisted. For example, $BaTiO_3$ is tetragonal. Both $SrTiO_3$ and $BaTiO_3$ with band gaps of 3.3 eV are interesting semiconductors for photoelectrolysis of water. Compared to $BaTiO_3$, $SrTiO_3$ has been more intensively studied.

Titanates with tunnel structures have been investigated for water splitting [17]. $BaTiO_9$ has a twin-type tunnel structure in which the TiO_6 octahedra are not parallel to one other, forming a pentagonal prism space. Alkaline metal hexatitanates ($M_2Ti_6O_{13}$; M = Na, K, Rb) have Wadsley-Andersson type structures in which TiO_6 octahedra share one edge at one level in linear groups of three, creating a tunnel structure with rectangular space. These materials have been used in powder form in suspensions, normally together with a co-catalyst.

There are more complex perovskites containing two different cations, which occupy either the A or B sites, and many of these have a layered structure. Two main classes of such oxides have been studied in water photolysis: the Dion-Jacobson series ($AM_{n-1}B_nO_{3n+1}$, e.g., $KCa_2Ti_3O_{10}$) and the Ruddlesden-Popper series ($A_2M_{n-1}B_nO_{3n+1}$, e.g., $K_2La_2Ti_3O_{10}$). Noble metal co-catalysts can be loaded onto these materials by photo deposition. Due to a negative charge (which is balanced by the alkali cations) of the oxide sheets, the noble metal salt anions will not be intercalated in the host lattice. Instead, the noble metal particles are formed on the external surfaces of the layered perovskites. In many cases, the H^+-exchanged layered oxides show higher activity for hydrogen production, due to the easy accessibility of the interlayer space to electron donor species [18, 19].

Another type of layered perovskite has the generic composition $A_nB_nO_{3n+2}$ ($n = 4, 5$; A = Ca, Sr, La; B = Nb, Ti). Unlike the (100)-oriented structures mentioned above, these perovskites have slabs parallel to (110) and are highly donor-doped. These structural and electronic characteristics are
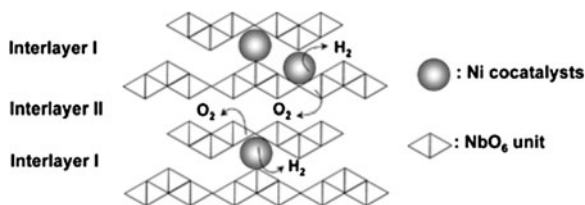
Fig. 5 Water splitting over $K_4Nb_6O_{17}$ photocatalyst with layered structure. From [5]. Reproduced by permission of The Royal Society of Chemistry (http://dx.doi.org/10.1039/b800489g)

thought to be responsible for the observed improved quantum yields for overall water splitting under UV irradiation. Among these compounds, $La_2Ti_2O_7$ (deduced from $La_4Ti_4O_{14}$) and $La_4CaTi_5O_{17}$ are representative titanates. Their band gaps are 3.2 and 3.8 eV, respectively, and they show quantum yields of 12% (< 360 nm) and 20% (< 320 nm), respectively [19, 20].

Tantalates and niobate oxides with corner-sharing octahedral MO_6 (M = Ta, Nb) structures have shown high photocatalytic activity for the cleavage of water. The high activity of these layered compounds can be assigned to the ease of migration and separation of photogenerated electron–hole pairs through the corner-shared framework of MO_6 units [21]. Tantalates, $MTaO_3$ (M = Li, Na, K) have been reported as effective photocatalysts for water splitting under UV irradiation. These oxides crystallize in perovskite structure, and their band gaps are 4.7 eV (Li), 4.0 eV (Na), and 3.7 eV (K) [22]. $NaTaO_3$ shows the highest photocatalytic activity among these $ATaO_3$ type photocatalysts when a NiO co-catalyst is loaded, which is due to the suitable conduction band level consisting of Ta 5d orbitals and energy delocalization caused by the small distortion of TaO_6 connections.

The layered oxides with ion-exchange characteristics have a net negative charge on the layered sheets. Thus, they can attract positively charged ions (such as K^+) in the interlamellar spaces. Interestingly, some of these materials (e.g., $K_4Nb_6O_{17}$) have two kinds of interlayers (I and II) that alternate, as shown in Fig. 5. H_2 is evolved from one interlayer, in which co-catalysts are introduced by ion-exchange or intercalation reactions, while O_2 production occurs in the other interlayer. In this case, the sites for H_2 and O_2 evolution are thus separated by the photocatalytic niobate sheet [5]. Furthermore, an electric field gradient originating from the uneven K^+ distribution on opposite sides of the niobate sheets assists electron–hole separation.

Generally speaking, oxides containing transition metal cations with d^0 electronic configuration like Ti^{4+}, Nb^{5+} or Ta^{5+} have wide band gaps (> 3.0 eV). Thus, these materials do not perform well under visible-light irradiation. The ternary and quaternary titanates, tantalates and niobates suffer from the same handicap. However, a series of H_2 production photocatalysts based on $K_4Ce_2M_{10}O_{30}$ (M = Ta, Nb) and their solid solution $K_4Ce_2Ta_{10-x}Nb_xO_{30}(x = 0 - 10)$ have appropriate band gaps of ca. 1.8–2.3 eV (corresponding to absorption edges of 540–690 nm)
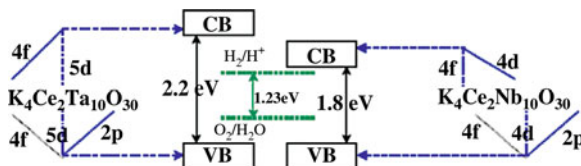
Fig. 6 Band structure of $K_4Ce_2M_{10}O_{30}$ (M = Ta, Nb) and comparison with redox couples for photocatalytic production of H_2 and O_2 from water. Reprinted from [23], Copyright 2007, with permission from, Elsevier (http://www.sciencedirect.com/science/journal/14686996)

[23, 24]. Density functional theory (DFT) calculations indicate that the valence bands of these photocatalysts are composed of hybridization with O 2p + Ta 5d (or Nb 4d) and occupied Ce 4f orbitals, while the conduction bands are mainly comprised of the Ta 5d (or Nb 4d) orbitals (Fig. 6). $K_4Ce_2M_{10}O_{30}$(M = Ta, Nb) has a parallelepiped (tunnel) surface structure. This is beneficial to the formation of "nano-nests", to which the co-catalysts, nanoparticles of Pt, RuO_2 and NiO_x, can be strongly associated, thus avoiding aggregation and improving photocatalytic H_2 generation greatly. This is an example of an effect of surface nanostructures on photocatalytic performance.

3.4 Metal Sulfides

Metal sulfides are considered attractive candidates for visible-light responsive photocatalysts. The valence bands of most metal sulfides consist of 3p orbitals of S, which results in a higher (more negative) valence band and narrower band gap compared to metal oxides.

Among the available metal sulfides, CdS with wurtzite structure is probably the most studied metal sulfide photocatalyst. Its narrow band gap (2.4 eV) means that it can absorb visible light below a wavelength of 510 nm. Compared to the VB of metal oxides being formed by O 2p orbitals, the VB of CdS is constituted by S 2p orbitals. The electronegativity of S is smaller than that of O, resulting in different VB positions. The CB potential of CdS is around -0.52 V (vs. NHE), high enough to reduce H_2O, and the top of its valence band is about 1.5 V (vs. NHE), suitable for the oxidation of H_2O. However, CdS is prone to photocorrosion (Eq. 4), which is a problem common to most metal sulfide photocatalysts.

$$2h_{VB}^+ + CdS = Cd^{2+}{}_{(aq)} + S_{(s)} \qquad (4)$$
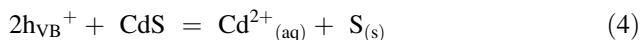
Many methods have tried to overcome this photocorrosion, such as combining with other semiconductors or using scavengers (electron donors, such as cysteines, EDTA, sulfide or sulfite species) to attract or consume photogenerated holes. In particular, H_2 generation from an aqueous medium containing S^{2-}/SO_3^{2-} is

appealing. H_2S is produced in large quantities as an undesirable by-product in coal- and petroleum-related industries, and similarly, sulfite is a pollutant. Thus, the combination of photo-oxidation of H_2S and/or sulfite (to sulfate), and co-generation of H_2 using CdS has a value-added benefit.

ZnS (zinc blende) is another important metal sulfide for photochemical water splitting. It shows high activity without any assistance of co-catalysts. It has a wide band gap of 3.6 eV, which restricts light absorption to the UV (< 340 nm). Studies have been carried out to sensitize ZnS. Doping and the formation of solid solutions are promising ways to improve the optical absorption of ZnS in the visible. Similar to CdS, it undergoes photochemical decomposition into the constituents when irradiated in the absence of sacrificial electron donors [25] (Eq. 5).

$$2h_{VB}^+ + \; ZnS \; = \; Zn_{(aq)}^{2+} + \; S_{(s)} \tag{5}$$
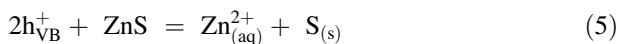
3.5 Metal Nitrides

We have seen that doping of nitrogen into the TiO_2 lattice has a favorable effect in terms of sensitizing it to the visible light range [26]. Reasonably, the band gap of Ta_2O_5 shrinks from ~ 4.0 to ~ 2.1 eV by nitriding it in a NH_3 atmosphere to yield Ta_3N_5. The shrinking of the band gap was attributed to a conduction band derived from Ta 5d orbitals and a higher-lying valence band derived from N 2p orbitals other than O 2p orbitals of Ta_2O_5. This material evolves H_2 and O_2 under visible irradiation (< 600 nm) in the presence of a sacrificial electron acceptor such as Ag^+ and a co-catalyst such as Pt [27].

Nitrides with d^{10} electronic configuration, such as Ge_3N_4 and GaN, are a new series of photocatalysts for the cleavage of water under UV-light irradiation. β-Ge_3N_4 exhibits the highest activity for the reaction among these nitrides. It is the first example of a non-oxide powdered photocatalyst for water splitting. The band gap of Ge_3N_4 is estimated to be 3.6–3.8 eV. The electronic structure of β-Ge_3N_4 was investigated using plane wave density functional theory (DFT) calculations. The density of states (DOS) indicate that the top of the valence band consists of N 2p orbitals, whereas the bottom of the conduction band is composed of hybridized Ge 4s4p orbitals. The band structure indicates that charge transfer under photo-excitation occurs from the N 2p orbitals to the hybridized Ge 4s4p orbitals. Because hybridized Ge 4s4p orbitals broadly expand, resulting from d^{10} electronic configuration, photogenerated electrons in such broad hybridized orbitals with large dispersion can be readily transferred to the co-catalyst, like RuO_2, on the surface without recombination, carrying out efficient overall water splitting [28]. The conduction band of GaN is 0.5 eV higher than the reduction potential of water, which is sufficient to overcome the over-potential for the release of hydrogen from a solution of methanol and Na_2S/Na_2SO_3 during the action of visible

light in the absence of additional co-catalysts [29]. The results for Ge_3N_4 and GaN indicate that broad hybridized sp orbitals with large dispersion in nitrides with d^{10} electronic configuration have suitable band structures for overall water splitting.

3.6 Oxynitrides and Oxysulfides

Oxynitride photocatalysts consisting of metal cations of Ti^{4+}, Nb^{5+} and Ta^{5+} with d^0 configuration are active for H_2 or O_2 evolution in the presence of sacrificial reagents. TaON has been found to be active for water oxidation and reduction under irradiation between 420 and 500 nm [30, 31]. Two other d^0 metal oxynitrides, $LaTiO_2N$ and $Y_2Ta_2O_5N_2$, were reported effective for evolving H_2 and O_2 from H_2O under visible-light irradiation [32, 33].

In the development of oxynitrides with d^{10} electronic configuration, a solid solution of GaN and ZnO, $(Ga_{1-x}Zn_x)(N_{1-x}O_x)$ was first tested for decomposing water under visible-light illumination [34]. The solid solution of ZnO and $ZnGeN_2$, $(Zn_{1+x}Ge)(N_2O_x)$ is another active d^{10} metal oxynitride photocatalyst for pure water splitting under visible light [35].

In addition to N, sulfur is another non-metallic element that has sensitized TiO_2 to visible light. Thus, oxysulfides have also been studied as potential photocatalysts for water splitting. $Ln_2Ti_2S_2O_5$ (Ln = Pr, Nd, Sm, Gd, Tb, Dy, Ho and Er) with layered perovskite structure was reported for photocatalytic water splitting. The band gap of this series of oxysulfides varies from 1.94 eV (Er) to 2.13 eV (Sm). $Sm_2Ti_2S_2O_5$ was found to have the highest activity among all the homologues tested [21, 36].

3.7 Other Materials for Photolytic H_2 Production

Group III–V semiconductors have several positive features that make them attractive for water splitting. The combination of high charge carrier mobility, an optimal band gap (particularly for many of the alloys) and reasonable photoelectrochemical stability of the *p*-type materials for cathodic H_2 production, should inspire continuing scrutiny of Group III–V semiconductors. As with their chalcogenide semiconductor counterparts, Group III–V semiconductors, in *n*-type form, undergo photoanodic corrosion instead of evolving O_2 under illumination in aqueous media. Fortunately, their *p*-type form is relatively stable against cathodic photocorrosion, and the photogenerated electrons on these *p*-type semiconductor cathodes can be used to reduce water to H_2, particularly in the presence of a co-catalyst such as Pt or Ru [37]. p-InP photocathodes are capable of evolving H_2 from HCl or $HClO_4$ electrolytes with very high efficiency [38]. Photocathodes

made from p-GaInP$_2$ (a solid solution of GaP and InP) biased with a GaAs p-n junction have also evolved H$_2$ with high efficiency [39].

Silicon has been studied for H$_2$ evolution under irradiation. One fundamental problem with Si from a water-splitting perspective is its low band gap (1.1 eV), which is too small for complete water splitting (1.23 eV). One way around this problem is to seek an alternative electron donor (e.g., ethanol, formic acid, HBr or HI), instead of water. For example, illumination of a Si powder photocatalyst whose anodic and cathodic surface were coated with polypyrrole and platinized Ag, respectively, caused hydrogen evolution from aqueous ethanol for longer than 150 h with a quantum efficiency of 2.1% at 550 nm [40]. Photocatalytic H$_2$ evolution from aqueous formic acid was successfully achieved by using platinized *n*-type silicon powder as a photocatalyst [41]. A tandem-type hydrogenated amorphous Si (a-Si) electrode having a [n-i-p-n-i-p] structure and a similar tandem a-Si electrode having [n-i-p-n-i-p] layers deposited on *p*-type crystalline Si showed cathodic photocurrents accompanied by H$_2$ evolution. These two electrodes, when connected to a RuO$_2$ counter-electrode (for O$_2$ evolution), caused sustained water splitting without external bias with solar-to-chemical conversion efficiencies of 1.98 and 2.93%, respectively [42].

CdSe nanoribbons show catalytic activity for photochemical hydrogen evolution from aqueous Na$_2$S/Na$_2$SO$_3$ solution under irradiation with ultraviolet and visible light [43]. This is one of few instances that displays the photocatalytic characteristics of CdSe, and the first evidence of the ability of CdSe to induce the reduction of water.

AgCl photoanodes combined with either p-GaInP$_2$ [44], or a single junction amorphous silicon solar cell connected to a platinum electrode [45] as the cathodic part of an electrochemical cell, split water. AgCl does not absorb light below the indirect-band gap transition, which is in the near-UV at about 3.3 eV (380 nm). The light sensitivity in the visible part of the spectrum is due to self-sensitization caused by reduced Ag species. The formation of these Ag clusters introduces new levels within the forbidden gap.

SiC was recently found to be able to reduce water upon exposure to visible light, even in the absence of electron-donating compounds [46].

4 Nanoscience and Nanotechnology Approaches Toward Improved Photolytic Water Splitting

Nature is a great source of inspiration, and the structure and function of both enzymes and the photosynthetic apparatus provide valuable guidelines for the design of optimized (photo) catalysts for water splitting. Key features of the biological analogues include: (i) judicious nanoscale design of reactant binding sites, (ii) ingenious arrangement of several components to form an electron transfer system and (iii) ultimate control of the reaction conditions by selectively operating transmembrane channels that connect the inside of a cell to the outside

environment. Researchers have tried to mimic some of these concepts in artificial catalysts with varying degrees of success. We will review some selected approaches, including methods to control charge separation and transport, attempts to steer the flow of reactants and products and means to confine the reaction volume. The potential benefits of these approaches will be discussed from the viewpoint of the issues associated with photochemical water splitting outlined in Sect. 2. Additionally, we will discuss nano approaches aiming to tune the light absorption properties.

4.1 Tuning of Electronic and Optical Properties

As outlined in Sect. 2 above, a mismatch between the solar spectrum and a semiconductor's absorption properties may severely limit the photoconversion efficiency under solar illumination. Approaches to modify the semiconductor's electronic band structure and thus optical absorption are therefore urgently needed and discussed below. Another factor limiting conversion efficiency is the fast recombination of photoexcited charge carriers. Various ways to minimize such recombination losses are therefore covered in this section.

4.1.1 Quantum Size Effects

The most interesting feature of semiconductor nanoparticles is the remarkable blue shift in their optical absorption spectra due to size reduction, compared to the corresponding bulk material. Molecular orbital (MO) and the linear combination of atomic orbitals coupled with molecular orbitals (LCAO-MO) procedures can provide information about energy level diagrams for clusters of several molecules (left part of Fig. 7) up to bulk semiconductors (right part of Fig. 7). Increasing the number of molecules in a cluster requires the addition of filled and empty orbitals to the energy manifold. This decreases energy differences between the filled orbitals and the empty orbitals. The energy gap between the highest occupied molecular orbital (HOMO) and the lowest unoccupied molecular orbital (LUMO) is also decreased. For a bulk semiconductor, the filled and empty states form separated continuums, i.e., the valence and conduction bands, respectively. In the Q-size regime, the energy levels within the filled and empty states remain discrete, and the gap between the HOMO and the LUMO states increases, compared to the bulk material, as shown in Fig. 7 [47]. This leads to a blue shift of the absorption edge in nanoparticles.

Accompanying the bandgap broadening due to reduced particle size, electrons at the lower edge of the conduction band and holes at the upper edge of the valence band then possess more negative and positive potentials, respectively. Therefore, electrons and holes have stronger reduction and oxidation powers, respectively, in such nanoparticles.
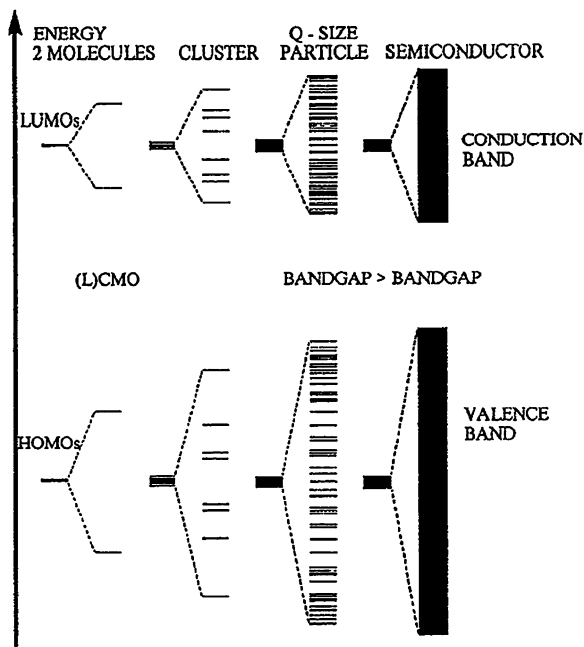
Fig. 7 Schematic diagram of the molecular orbital model for band structure. The number of energy levels increases with increasing number of atoms in the cluster. This results in a decrease in spacing within the occupied and unoccupied levels, and between the HOMO and LUMO levels. For bulk crystals the states within the occupied and unoccupied levels are so close that it is convenient to represent them as separated bands, i.e., the valence and conduction bands. The energy gap between these bands is the band gap, E_g, which increases in magnitude as the semiconductor particle radius decreases to the point where it becomes comparable to or smaller than the exciton radius. Reprinted from [47]. With kind permission from Springer Science + Business Media: Fig. 8

4.1.2 Modification by Doping

As mentioned above, semiconductors with a wide bandgap have stronger reduction and oxidation power. However, the main drawback of a large bandgap is the low utilization of solar light. For single semiconductor systems, dye sensitization has shown some encouraging results. It is, however, not easy to find a suitable and stable dye that can be illuminated over extended periods of time. Another way to sensitize semiconductors is by doping with ionic species. Although in many cases a red shift of the absorption edge into the visible region is observed in doped semiconductors, it should be noted that the photocatalytic activity may not necessarily increase under visible-light irradiation, since the measured absorption spectra of doped semiconductors result from several absorption transitions of different origins. Since the effects of doping depend on many factors, including the
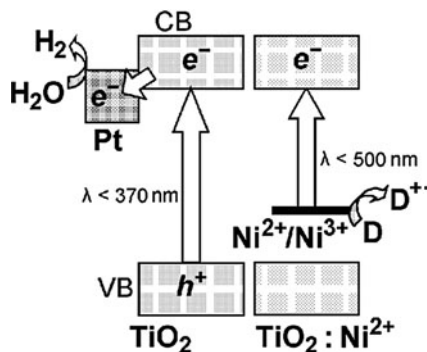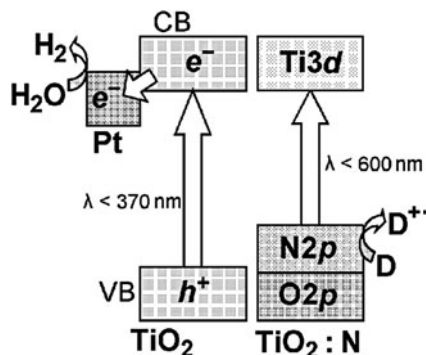
Fig. 8 Energy diagram of the operation of a photocatalytic system for the release of hydrogen from an aqueous solution containing an electron donor D for undoped titanium dioxide (LHS) and titanium dioxide doped with Ni^{2+} (TiO_2:Ni^{2+}, RHS). From [48]. With kind permission from Springer Science + Business Media, Fig. 3

doping method, the dopant species, the amount of dopant and the distribution of dopant in the semiconductor matrix, the role and behavior of dopants are still not completely clear and need to be investigated further.

The doping of wide-band gap semiconductors with transition metal ions creates local states (new energy levels) within the forbidden band. Visible-light absorption and photoactivity are induced by the interband, as shown in Fig. 8. Here, water is reduced by the photogenerated electrons, while the dopant metal ions get back electrons from a donor. This induced visible-light photoactivity is normally low, due to the small amount of visible-light absorption, as indicated by a small shoulder in the visible-light region, instead of a total red shift of the absorption edge. Increasing the dopant concentration in the semiconductor matrix can improve visible-light absorption, but excessive doping can easily disturb the original structure. Sometimes, doping can extend the lifetime of photogenerated charge carriers by trapping them transitorily and shallowly. On the other hand, dopants can also act as recombination centers for photogenerated electrons and holes and decrease photocatalytic activity.

Doping semiconductors with non-metal ions can also form intra-bandgap energy levels, as in the case of transition metal doping. For example, doping TiO_2 with F^- forms new energy states (color centers) close to the conduction band of TiO_2 (0.53 eV below the conduction band edge of TiO_2 for F center and 0.84 eV for F^+ center), resulting in an enhanced photocatalytic activity of TiO_2 under both UV and visible-light irradiation [49]. N-doping can locate N 2p states near the top of the valence band of TiO_2, which was predicted by theoretical calculations [50] and confirmed by photocatalytic experiments [51]. Interestingly, anionic doping of semiconductors with suitable N, C or S concentration can also narrow the bandgap due to mixing of the p orbitals of the dopant and oxygen, as shown in Fig. 9. The concentration should be higher than that required for the formation of discrete p

Fig. 9 Energy diagram of the operation of a photocatalytic system for the release of hydrogen from an aqueous solution containing an electron donor D for undoped titanium dioxide (LHS) and nitrogen-doped titanium dioxide (TiO$_2$:N, RHS). From [48]. With kind permission from Springer Science + Business Media, Fig. 4

states of dopants, which are close to the valence band. The dopant p orbitals then contribute to the top of the valence band, while the bottom of the conduction band is still formed by transition metal d orbitals without any change. Although some fruitful results have been achieved by this approach, it is difficult for a semiconductor to maintain its electronic balance and structural stability after incorporating large amounts of dopants. Heavily-doped oxides are non-stoichiometric and contain too many oxygen defects, due to different oxidation numbers of oxygen and dopants. These defects will reduce photocatalytic activity. Furthermore, excessive N (or S) doping can also change the structure of doped samples to stoichiometric oxynitrides (oxysulfides) or even nitrides (or sulfides), which, in many cases, are not very photoactive (there are also some exceptions, as mentioned in previous Sects. 3.4–3.6). The stability of dopants during long-term photocatalytic H$_2$ production should also be considered, since the bonds between transition metals and dopants are normally weaker than those between transition metals and oxygen, due to the smaller electronegativity of dopants as compared to oxygen.

4.1.3 Modification by Nanostructured Co-catalysts

Nanostructured co-catalysts, traditionally based on noble metals, have been widely investigated and used in photocatalytic systems for H$_2$ production. The function of these co-catalysts is to shuttle photogenerated electrons from the semiconductor to an acceptor (H$^+$ for H$_2$ production) in a photocatalytic process. Besides noble metals, co-catalyst chemistries also include nickel and its oxide, the mixed oxides of rhodium and chromium, tungsten carbide, MoS$_2$ and so on. The promoting mechanism of co-catalysts is illustrated in Fig. 10. Under irradiation by photons with enough energy (equal to or larger than the semiconductor bandgap), photogenerated electrons are promoted from the valence band to the conduction band of
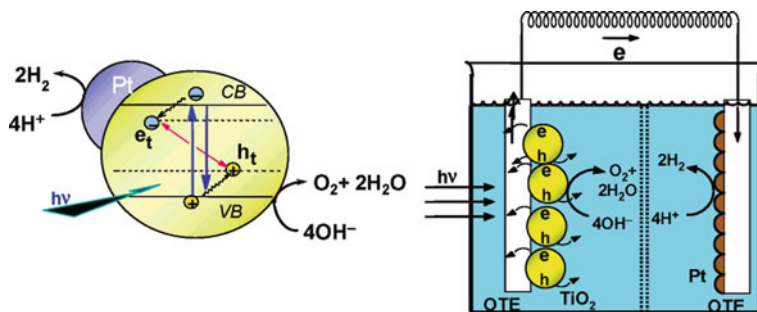
Fig. 10 Splitting of water by photocatalyst nanoparticles modified with Pt co-catalyst nanoparticles (LHS) and in a photoelectrochemical cell based on a nanostructured TiO_2 film anode and a nanostructured Pt cathode (RHS). Reprinted with permission from [52], Copyright 2007 American Chemical Society

the semiconductor, which raises the Fermi level of the semiconductor. Then, the energy difference at the semiconductor/metal interface drives electrons from the conduction band of the semiconductor to the noble-metal nanoparticle. The Fermi level of the noble-metal is thereby negatively shifted, which drives another electron transfer to an electron acceptor (H^+ in the case of H_2 production). This concept is also applicable to photoelectrochemical cells for H_2 production. Instead of a direct contact as in particulate photocatalysis, in photoelectrochemical water splitting, a noble metal counter-electrode (cathode) is connected to the semiconductor photoanode by an external circuit, which leads to spatial separation of H_2 and O_2 evolution sites and thus has the additional benefit of restraining their back-reaction to water (as shown on the RHS of Fig. 10).

One of the early studies indicated how different noble metals influence semiconductor-based photocatalytic H_2 production [53]. A direct correlation between the work function of the noble metals and the photocatalytic activity was also studied for metalized TiO_2 photocatalysis systems [54]. Besides the species of noble metal, the size of the noble-metal nanoparticle also largely affects the energetics and the electron transfer between the semiconductor and noble metal by shifting the Fermi level to more negative potential for smaller sizes. In the TiO_2-Au system, higher photocatalytic reduction efficiency was obtained with smaller Au nanoparticles [55]. Identifying and developing less expensive (noble) metals (like Ag) as co-catalysts for solar H_2 production is an important research topic.

4.1.4 Coupling to Another Nanostructured Semiconductor

Photoinduced charge separation can be realized by coupling one semiconductor with another. Matching their conduction and valence band levels can drive a vectorial transfer of photogenerated charge carriers from one semiconductor to the other, thus minimizing losses via electron–hole recombination. A case of special

Fig. 11 Diagram illustrating spatial separation of photogenerated charge carriers in a CdS/TiO$_2$ heterostructure and the formation of hydrogen during the action of visible light. From [48]. With kind permission from Springer Science + Business Media, Fig. 2
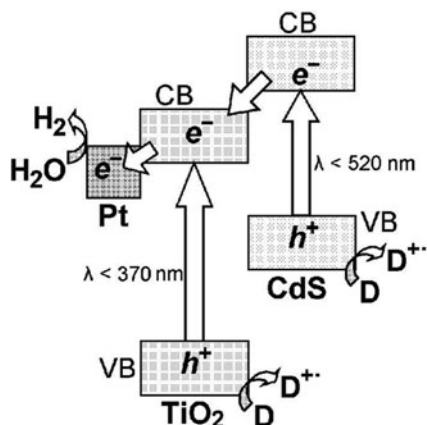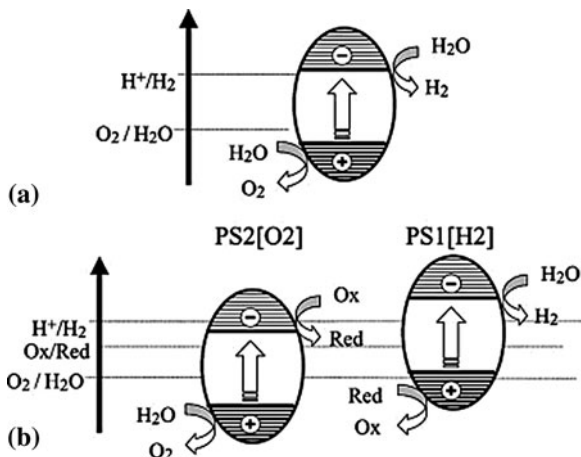

interest is to select a narrow bandgap semiconductor as a coupling semiconductor in order to realize harvesting of visible light. Semiconductors, such as CdS, PbS, Bi$_2$S$_3$, CdSe and InP that can absorb visible light serve as sensitizers in semiconductor/semiconductor nanocomposites because they are able to transfer photogenerated electrons to wide-bandgap semiconductors, such as TiO$_2$, ZnO and SnO$_2$, as illustrated in Fig. 11. The band structure of two coupled semiconductors and the photogenerated charge transfer between them are determined by many factors, such as particle size, crystal structure, crystallinity, defect type and density and surface area; by tuning these factors, the flow of charge carriers can be adjusted and lead to enhanced photocatalytic and photoelectrochemical performance of such coupled-semiconductor systems. For example, the energetics can be controlled by varying the size of the semiconductor quantum dots. Increasing the band energies of these quantum dots was utilized to promote, suppress or rectify the electron transfer between two semiconductors [52].

In a traditional photocatalytic water-splitting system, semiconductor photocatalysts should possess both conduction band and valence band potentials that are suitable for H$_2$ and O$_2$ evolution, respectively, as shown in Fig. 12a. This requirement seriously limits photocatalyst selection and visible-light utilization. A Z-scheme photocatalytic water-splitting system, which involved two-step photoexcitation under visible-light irradiation, was developed by mimicking the natural photosynthesis of green plants [56]. The Z-scheme system consisted of a H$_2$-evolution photocatalyst (PS1 in Fig. 12b) an O$_2$–evolution photocatalyst (PS2 in Fig. 12b) and a reversible redox mediator (Ox/Red) that acted separately as the electron donor (for PS1) and acceptor (for PS2) for the respective half reactions.

Photocatalysts, which alone are only effective in one of the two half reactions in water splitting, are capable of running both half reactions when arranged in a Z-scheme. SrTiO$_3$, TaON, CaTaO$_2$N and BaTaO$_2$N can work as H$_2$ evolution photocatalysts, while WO$_3$, BiVO$_4$ and Bi$_2$MoO$_6$ can act as O$_2$ evolution photocatalysts. The IO$_3^-$/I$^-$ and Fe^{3+}/Fe^{2+} redox couples normally serve as reversible electron mediators. An all-solid-state Z-scheme based on a CdS–Au–TiO$_2$

three-component nanojunction was recently reported, where PS1(CdS), PS2(TiO$_2$) and the electron-transfer system (Au) were spatially fixed [57]. The vectorial electron transfer of $TiO_2 \rightarrow Au \rightarrow CdS$ occurs as a result of excitation of both TiO_2 and CdS. The electron supply from TiO_2 to CdS via Au restricts the self-decomposition of CdS due to the oxidation of surface S^{2-} ions by the photo-generated holes in CdS. In a Z-scheme system, H_2 and O_2 are evolved separately by two different photocatalysts, which, to some extent, restrains their back-reaction to water. The key factors in the design of a Z-scheme system are to find a pair of photocatalysts for separate H_2 and O_2 production with high efficiency, and a reversible electron mediator, the redox potential of which can meet the requirements of being electron donor and acceptor in the respective half reactions. From what we have mentioned above, the energy levels of the components and charge transfer between them should be considered when designing both semiconductor–semiconductor nanocomposites and Z-scheme systems.

4.2 Micro- and Nanostructures for Light Management

An important issue in photovoltaic and photolytic energy conversion is a large mismatch between optical and electronic length scales for photon energies close to the semiconductor bandgap; while the absorption depth of light is on the order of (hundreds of) micrometers, the electronic diffusion length is at least an order of magnitude smaller. The optimal device thickness is thus a compromise between absorbing most of the incoming photons and reducing volume recombination of excited charge carriers. Ideally, one would like to construct optically thick but physically thin absorbers. This concept provides several advantages, including resource-efficient use of (in certain cases expensive and/or scarce) materials, the

opportunity to use relatively impure materials and/or the potential to achieve higher device efficiency.

While various approaches to address this issue have been presented in the context of photovoltaic (PV) solar cells, our opinion is that their usefulness for photochemical energy conversion, and in particular photochemical water splitting, has not yet been exploited fully. Much of the work reviewed in this section is therefore taken from the area of photovoltaics, with a strong belief that the presented schemes are of high relevance also for photochemical water splitting.

Traditional light-trapping approaches in PV solar cells include the use of wavelength-scale textured substrates [58] and diffractive optical structures [59], which can increase the optically effective cell thickness by a factor of 4–5. More recently, light-scattering layers [60] and optical microcavities [61], including photonic crystals [62, 63] and whispering gallery modes, have attracted significant interest. The latter is named after the whispering gallery at St. Paul's Cathedral in London and occurs at particular resonant wavelengths of light for a given cavity size and shape when the light undergoes total internal reflection at the inner surface and becomes trapped within the void (or guide) for timescales of the order of nanoseconds [64]. Obviously, the increased photon path length increases the total absorption. An illustrative example of this effect is the observation of photolysis of water-soluble components inside cloud droplets by ultraviolet/visible radiation [65]. Most photonic dielectric cavities have traditionally been limited to sizes that are in the order of the wavelength of light. The lower bound on the effective mode volume (V_{eff}) arises from a mechanism of confinement based on interference effects and is therefore wavelength dependent. However, it has been shown [66] that by introducing dielectric discontinuities with sub-wavelength dimensions as a means of local field enhancement, the effective mode volume becomes wavelength independent. In this way cavities with large V_{eff} can be achieved, with a corresponding increase in the Purcell factor (a measure of the spontaneous emission rate enhancement for an emitter in a resonant cavity) of nearly two orders of magnitude relative to previously demonstrated high index photonic crystal cavities.

The most recent development in the area of light management for solar energy applications involves the utilization of plasmonically-active nanostructures. It is well-known that nanoparticles and perforated films of certain materials (e.g., silver, gold, platinum) show strongly enhanced optical absorption (i.e., increased cross-section for initial photon capture) due to the excitation of localized surface plasmon modes [67, 68]. Localized surface plasmon resonances (LSPRs) are collective oscillations of the conduction electrons, which may result in optical absorption cross-sections that exceed the geometric cross-section by several orders of magnitude. These plasmons are accompanied by a strongly enhanced electromagnetic near field. They may decay either radiatively (i.e., by re-emitting a photon), or non-radiatively into (quasi) particles such as electron–hole (e–h) pairs. For many metals, the resonance wavelength falls into the near-ultraviolet, visible or near-infrared regime for nanostructure sizes covering the range 20–200 nm. What is typical for the mentioned spectral range is that it covers (most of) the energetics of

important chemical transformations, e.g., bond breaking and bond formation (0.5–6.5 eV). This should allow one to create conditions and propose schemes for enhanced (solar) light absorption in nanostructured materials and utilization of the deposited energy to run chemical transformations such as water splitting.

There are various pathways along which plasmonics may enhance solar-cell devices, as summarized in a recent review by Atwater and Polman [69]. In short, plasmonic structures can function as: (i) scattering structures that couple freely propagating waves from the sun into (waveguiding modes in) a thin semiconductor absorber layer (see [70, 71]), (ii) light-trapping structures, which effectively bend the incoming solar flux by 90° via the excitation of propagating surface plasmon polaritons (SPPs) [72, 73] and (iii) nanoantennas that increase the absorption in the adjacent semiconductor via their strongly enhanced plasmonic near-field [74, 75]. In the first two cases, the effective path length of the incident light in the semiconductor is increased, whereas in the final case, the incident light is concentrated into nanoscale volumes around the plasmonic nanoparticles. Experimental and theoretical work indicate that the active layer thickness of various types of solar cells, including organic solar cells, dye-sensitized solar cells and inorganic solar cells, may be decreased by 10–100-fold using such schemes with no significant impact on efficiency. While the three radiative pathways described above have shown great potential for PV devices, a potential fourth pathway, namely (iv) charge carrier generation via non-radiative plasmon decay has not been investigated to the best of our knowledge, and its usefulness for photovoltaic power generation thus remains to be shown.

Finally, we note that there are a number of recent design suggestions based on nanostructures that do not involve plasmonic effects. To mention a few, Kelzenberg and colleagues [76] demonstrated the use of microrod arrays in between which light is scattered and Zhu et al. [77] recently introduced nanodome solar cells.

In the case of plasmon-enhanced photochemistry, an area pioneered by Nitzan and Brus in the early eighties [78], both radiative and non-radiative enhancement pathways have been pursued, as illustrated in an extensive review article by Watanabe et al. [79]. To give two representative examples, the photocatalytic degradation of methylene blue was found to be significantly increased on nano-composite photocatalysts consisting of silver nanoparticles embedded in titania. Radiative energy transfer from the Ag nanoparticles to the semiconductor was claimed to be the origin of the increased efficiency [80, 81]. Tian and Tasuma, on the other hand, reported that ethanol and methanol were photocatalytically oxidized by gold nanoparticle–nanoporous TiO_2 composites (at the expense of oxygen reduction) under visible-light illumination [82]. In this case, photoexcitation of the gold nanoparticles was followed by simultaneous charge transfer of electrons from the gold to the TiO_2 conduction band and from a donor in the solution to the gold nanoparticle, as illustrated in Fig. 13.

While the traditional light-trapping schemes presented at the beginning of this section seem to be primarily interesting for photoelectrochemical water splitting, the discussed plasmonic amplification schemes are applicable to both PEC and

Fig. 13 Schematic illustration of charge separation at an illuminated gold nanoparticle–titania interface, enabling visible-light induced photocatalytic oxidation of alcohols. Reprinted with permission from [82]. Copyright 2005 American Chemical Society
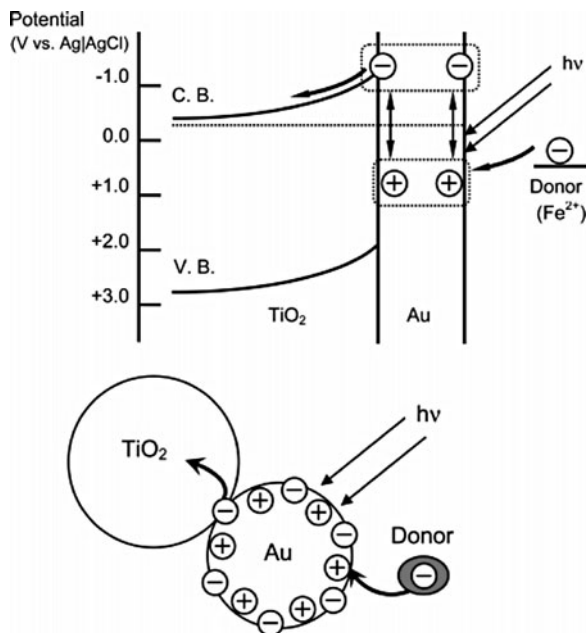
photocatalytic water splitting. Despite a large potential, we are not aware of any actual realizations of plasmon-enhanced water splitting.

4.3 Control of Photocatalyst Structure and Morphology

Structure and morphology are important and hot issues in photocatalysis, since both affect the performance of a photocatalytic material. Small size and large surface area normally correspond to high photocatalytic activity. Low-dimensional nanostructures with high aspect ratio and porous nanostructures have attracted intense attention, since they favorably affect charge and mass transport, respectively.

4.3.1 Small Size and Big Surface Area: Catalytic and Photocatalytic Considerations

Heterogeneous catalysis is dependent on processes taking place at surfaces and interfaces. Since catalytic materials are often expensive, the goal has always been to fabricate catalysts with the highest possible surface-to-volume (S/V) ratio. In real-life catalysts, this is usually achieved by depositing small (< 5 nm), catalytically active nanoparticles onto a highly porous support material with very high surface

area [83]. In parallel, it is known that nanostructures may possess catalytic power not found in their bulk counterparts. As an example, it was shown that tiny dots of gold on certain metal oxide supports exhibit extraordinary catalytic properties, despite the fact that bulk gold is chemically inert [84].

Similar to "normal" (dark) heterogeneous catalysis, the size of photocatalyst particles determines the surface area available for the adsorption and decomposition of reactants (e.g., water or H_2S in H_2 production), and for the harvesting of light. Besides providing more active sites due to large surface area compared to their bulk counterparts, nanosized photocatalysts can restrain bulk electron–hole recombination via charge-carrier trapping on their way to the surface. Photogenerated electrons and holes need to diffuse to the photocatalyst surface to react with electron and hole acceptors (reactants). If the dimensions of nanosized photocatalysts are small enough so that the transfer of photogenerated electrons and holes to the surface is faster than the recombination process, the photocatalytic efficiency will be largely enhanced. It should be noted, however, that the photocatalytic activity does not always increase with decreasing photocatalyst size. There are several potential disadvantages if the size becomes too small. First, too small a size cannot guarantee the best crystal structure for photocatalysis. Normally, very small particles (or quantum dots) are more prone to have amorphous structure. Secondly, very small particles easily aggregate. The size and morphology of these aggregates, or secondary particles, can affect the light-scattering properties of the photocatalyst, as well as the degree of photon penetration. The slow transport of reactants and products within the aggregates can also decrease the photocatalytic efficiency [85]. Finally, particles that are too small may result in increased surface electron–hole recombination, which offsets the benefits of high surface area. It is believed that there are respective optimal sizes at the nanoscale for different photocatalytic materials and reactions.

### 4.3.2 1-D Nanostructures: Nanowires, Nanorods, Nanotubes and Nanofibers

One-dimensional (1-D) nanostructured materials (nanowires, nanorods, nanotubes and nanofibers) have attracted more and more attention due to their specific properties, which differ from the bulk and other nanostructure (nanoparticle) counterparts. Compared to a nanoparticle with the same volume or weight, a 1-D nanostructure can provide higher surface area and faster interfacial charge transfer rate. As shown in Fig. 14, photoelectrodes composed of nanorods oriented perpendicular to the conductive substrate (see Fig. 14b) can shorten the transport distance for electrons to the back contact (the "electron expressway" concept [86]) and avoid recombination losses at grain boundaries between nanoparticles (see Fig. 14a) [87].

Furthermore, poor hole transport has been known to be one of the main factors that limit the conversion efficiency of Fe_2O_3 photo anodes. An elegant solution for this is to use high aspect-ratio nanowire electrodes. It was reported that the

Fig. 14 Schematic representation of the electron transport through (**a**) spherical particles and (**b**) nanorods with preferential orientation. From [87]. Reproduced by permission of The Electrochemical Society
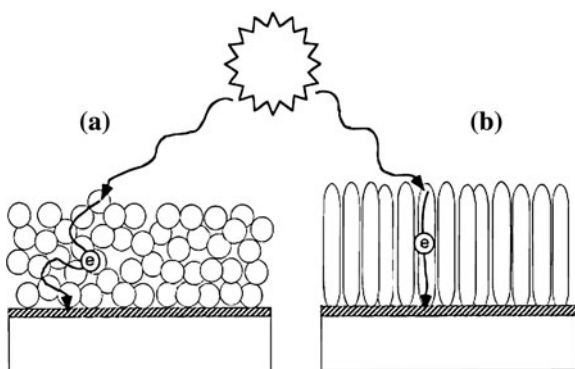

Fig. 15 Optimized morphology for an α-Fe_2O_3 photo-anode for water splitting. The small diameter of the nanowires ensures short hole diffusion path lengths. From [88]. Reproduced by permission of The Royal Society of Chemistry, http://dx.doi.org/10.1039/B718969A
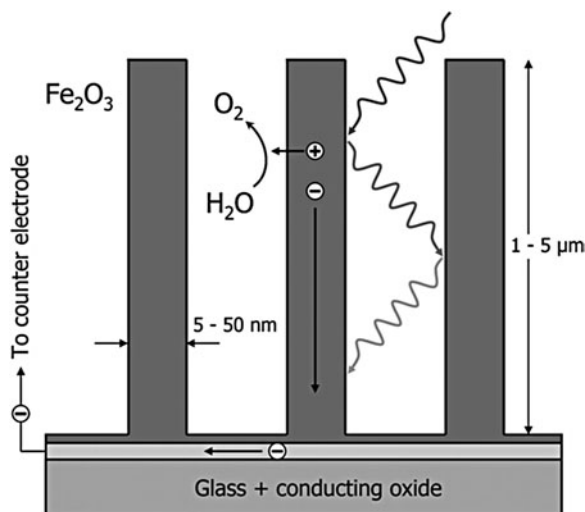
transport distance for photogenerated holes to the Fe_2O_3–electrolyte interface was reduced in Fe_2O_3 nanowires with a small diameter, as illustrated in Fig. 15 [88]. One can imagine that the limitation with regard to hole transport can be overcome when the radius of the Fe_2O_3 nanowires is smaller than the hole diffusion length.

It should be noted that even with the same 1-D morphology of the basic building blocks, disorder, order and different orientations of the 1-D units affect the photoelectrochemical properties. As shown in Fig. 16, the photon-to-current efficiency is lower for the Fe_2O_3 electrode with nanorods parallel to the substrate. The IPCE at 360 nm is 3% compared to 5% with nanorods oriented perpendicularly. The electrons have a more straightforward pathway to the back contact with nanorods perpendicular to the substrate, which leads to a decrease in recombination losses (see Fig. 16b) and higher IPCE values [87].
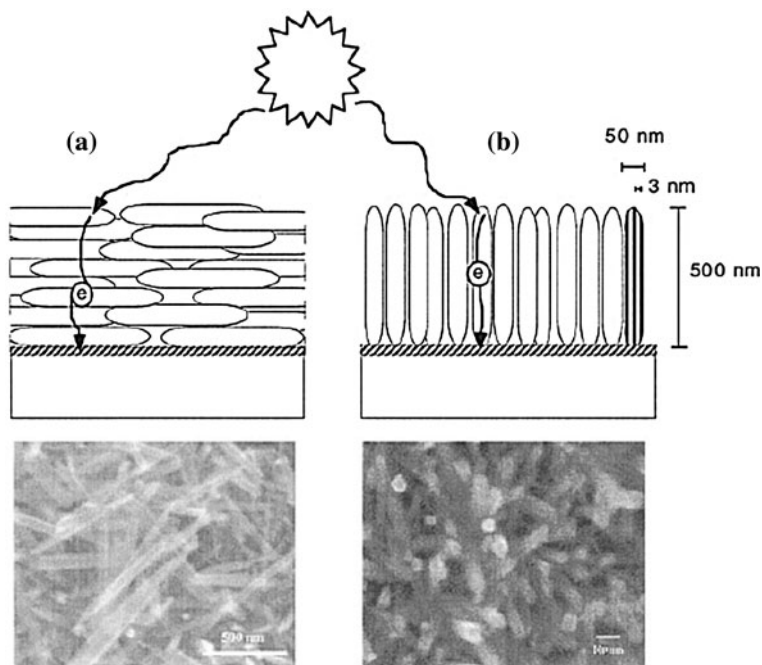
Fig. 16 Schematic illustration (*cross-section*) and scanning electron micrograph (*top view*) of hematite nanorods with (**a**) parallel and (**b**) perpendicular orientation to the conducting substrate. From [87]. Reproduced by permission of The Electrochemical Society

We additionally note that the basic concepts described above also hold for more complex nanostructures, such as the Fe_2O_3 "cauliflower" structure reported by Kay et al. [89].

Although the initial idea of using 1-D nanostructured (nanorod) electrodes for PEC water splitting was first reported for Fe_2O_3 [90], it has been widely investigated using other semiconductor electrodes, including novel materials such as VO_2 [91] and Ta_3N_5 [92], and, especially, TiO_2 (see [93] for a recent review). Thin film and nanowire electrodes of *n*-type titanium oxide (n-TiO_2) were fabricated and their photoresponse toward water-splitting was measured; a more than twofold increase in maximum photoconversion efficiency was observed when a single-layer thin film of n-TiO_2 was replaced by nanowires [94]. Photoelectrochemical water splitting using dense and aligned TiO_2 nanorod arrays with well-defined length was also reported; overall water splitting was observed with an applied overpotential of 1.0 V (versus Ag/AgCl) with a photon-to-hydrogen efficiency of 0.1%. The results suggest that these dense and aligned one-dimensional TiO_2 nanostructures are promising for hydrogen generation from water by PEC cells [95]. The concept of using 1-D nanostructures for H_2 production via PEC water splitting has also been extended to nanotubes. Compared to nanorods and

nanowires, nanotubes have higher surface area for redox reactions. Highly ordered titania nanotube arrays of variable wall thickness were used to photocleave water under ultraviolet irradiation. It was found that the nanotube wall thickness is a key parameter influencing the magnitude of the photoanodic response and the overall efficiency of the water-splitting reaction. Using nanotubes with a 22 nm porediameter and 34 nm wall thickness, upon $320 - 400$ nm illumination at an intensity of 100 mW/cm^2, hydrogen was generated at a rate of 960 μmol/h W (24 mL/h W) and an overall conversion efficiency of 6.8%, which was the highest value reported for a titania-based photoelectrochemical cell [96].

Besides the application in PEC H$_2$ production, 1-D nanostructures also play a very important role in photocatalytic H$_2$ production. TiO$_2$ nanotubes modified with Pt were found to be a photocatalytic dehydrogenation catalyst in neat ethanol for producing H$_2$ gas [97]. Self-organized TiO$_2$ nanotube-layers were fabricated by electrochemical anodization of Ti in a HF electrolyte, and then Pt was deposited on the TiO$_2$ nanotube layer by plasma sputtering. The Pt-TiO$_2$ nanotube photocatalyst generated H$_2$ successfully from an alkaline water solution [98]. Pt-ionized TiO$_2$ nanotubes were prepared for the stoichiometric production of H$_2$ and O$_2$ by water-splitting under visible light with hydrogen evolution rates of 14.6 and 2.3 μmol/h in aqueous methanol and pure water, respectively [99]. Nanostructured TiO$_2$ films with controlled morphology and thickness were synthesized for use in water splitting photocells and dye-sensitized solar cells. Two different morphologies were compared: a granular morphology and a highly crystalline columnar morphology. The columnar morphology outperformed the granular morphology for both applications, achieving a UV-light to hydrogen conversion efficiency of 11% for water splitting, and a visible light to electricity conversion efficiency of 6.0% for the dye-sensitized solar cell [100]. TiO$_2$ nanowires (TiO$_2$ NWs) were synthesized through a one-step hydrothermal process followed by post heat treatment. In this study, anatase TiO$_2$ NWs exhibited the highest photocatalytic H$_2$ evolution, which was also higher than that of the starting TiO$_2$ powder (Degussa P25) [101]. However, Lin et al. suggested that a bi-crystalline structure consisting of TiO$_2$ (B) nanotubes (or nanofibers) and anatase nanoparticles could act as an active, H$_2$-producing photocatalyst [102, 103]. A solvothermal method was applied to synthesize CdS nanorods [104] and nanowires [105], which have high photocatalytic activity for H$_2$ production.

We finally note that the concepts of 1-D nanostructured materials and semiconductor–semiconductor nano-composites, as discussed in Sect. 4.1.4, can be combined and lead to synergistic effects [106]. The same holds for the deposition of co-catalyst nanoparticles (Sect. 4.1.3) onto 1-D nanostructured materials, which leads to improved charge separation properties [107, 108]. Qu et al. demonstrated the fabrication of rationally designed 1-D nanostructures, which integrate several concepts in a single nanosystem. The combination of a charge-separating nanodiode structure, which was encased in a protective insulating shell and functionalized with two exposed metal co-catalysts, was both highly efficient and stable throughout the entire solar spectrum [109].

4.3.3 2-D Nanostructures: Nanosheets, Nanoscrolls and Layered Materials

From the microstructure point of view, nanosheets, nanoscrolls and layered materials belong to two-dimensionally (2-D) structured materials. For photocatalytic H_2 production, 2-D structured materials can maintain a high surface area, selectively expose certain photocatalyst facets with high photocatalytic activity, provide fast charge transfer and stack multicomponent structures by layer assembly.

Photocatalytic H_2 production over Pt/TiO_2 nanosheets with exposed (001) facets was reported recently [110]. The authors concluded that the exposed (001) facets contributed largely to the high photocatalytic activity in H_2 production, which was also proven by Lu et al. [111, 112]. In a dye-sensitized semiconductor photosystem, the semiconductor particle mediates electron transfer between the dye and a particle catalyst for hydrogen evolution (typically Pt or Rh). For the reaction to be efficient, the rate of electron transfer to this catalyst must be faster than that of back electron transfer to the oxidized dye or electron donor. Oxide nanosheets make particularly good electron transfer mediators. An external quantum yield of 20–25% was observed for hydrogen evolution from $EDTA^{2-}$ solutions with niobate nanoscrolls and nanosheets catalyzed by Pt and sensitized by a phosphonated $[Ru(bpy)_3]^{2+}$ derivative (Fig. 17). Taking into account light scattering, the low extinction coefficient of the dye, and the charge injection efficiency, this system has > 50% internal quantum yield for hydrogen evolution from photoinjected electrons. This high internal quantum yield shows that the single-crystal oxide nanoscrolls and nanosheets are good mediators of electron transfer between the dye molecules and Pt particles. Since the electron transfer from $EDTA^{2-}$ to Ru^{3+} was the slowest (limiting) step in the overall reaction, these results demonstrate that the nanosheet morphology was largely responsible for the enhanced overall photon conversion efficiency [113].

Layered structures have been widely used in photocatalytic H_2 production. $K_4Nb_6O_{17}$ has a layered structure with two kinds of interlayers. H_2 is evolved from one interlayer, in which co-catalysts are introduced by ion-exchange or interlayer reaction, while O_2 is produced in the other interlayer, as shown in Fig. 18. In this way, the sites for H_2 and O_2 evolution are separated by the photocatalytic niobate sheet [5]. Furthermore, an electric field gradient resulting from the uneven K^+ distribution on opposite sides of the niobate sheets assists electron–hole separation.

4.3.4 Porous Structures

Porous materials, behaving as spatially confined micro- and nanoreactors (see Sect. 4.4.2 below for further details), have attracted more and more attention in photocatalysis. They have high surface areas, and they can concentrate reactants with low concentrations, control the reaction environment and provide host–guest effects. Selective photocatalysis can be realized by adjusting the pore size. Co-catalysts can be easily deposited and dispersed onto these porous

Fig. 17 (*Top*) Schematic representation of photo-induced electron transfer from a phosphonated [Ru(bpy)$_3$]$^{2+}$ sensitizer to Pt catalyst particles, mediated by H$_4$Nb$_6$O$_{17}$ nanoscrolls. (*Middle*) TEM images of individual nanosheets and of nanoscrolls precipitated from a suspension of exfoliated H$_4$Nb$_6$O$_{17}$. (*Bottom*) The dependence of hydrogen evolution rate on Pt loading and the observed high quantum yield establish that electron transfer from EDTA^{2-} to Ru^{3+} is the slowest step in the overall process. Reprinted with permission from [113]. Copyright 2009 American Chemical Society
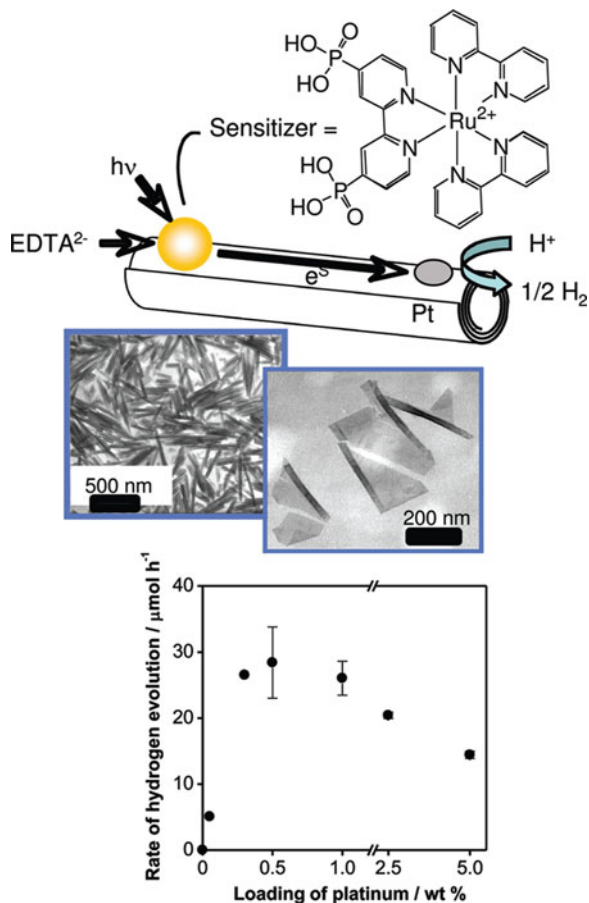
photocatalysts. Peng et al. reported that hydrothermally synthesized TiO$_2$ nano-particles without calcination had a large specific surface area (438 m^2/g) with small crystallites (2.3 nm) dispersed among amorphous mesoporous domains, and exhibited much better photocatalytic activity for H$_2$ production compared to samples calcined at different temperatures and also the commercial photocatalyst P25 [114]. A novel synthesis was carried out using KCl electrolyte to control the electrostatic repulsive force between TiO$_2$ nanoparticles toward the formation of a mesoporous structure, which owned the highest photocatalytic activity for H$_2$ production, compared to nonporous colloidal-TiO$_2$, and commercial Degussa P25 and Hombikat UV-100 (HBK) samples [115]. The photocatalytic reduction of metal cations (M = Ni^{2+}, Co^{2+}, Cu^{2+}, Cd^{2+}, Zn^{2+}, Fe^{2+}, Ag$^+$, Pb^{2+}) on the surface of mesoporous TiO$_2$ (specific surface area 130–140 m^2/g, pore diameter 5–9 nm, and anatase content 70–90%) resulted in the formation of nanostructured metal–semiconductor composites (TiO$_2$/M). These metal–TiO$_2$ nanostructures showed a remarkable photocatalytic activity for hydrogen production from water–alcohol
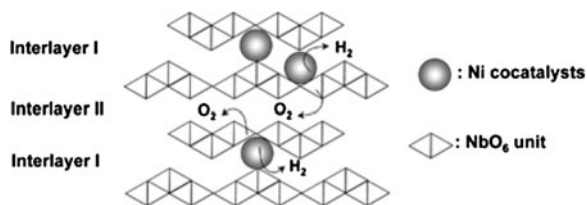
Fig. 18 Water splitting over $K_4Nb_6O_{17}$ photocatalyst with layered structure. From [5]. Reproduced with permission from The Royal Society of Chemistry (http://dx.doi.org/10.1039/b800489g)

mixtures, and the efficiency was 50–60% greater than that of the metal-containing nanocomposites based on Degussa P25. The anatase content and pore size proved to be the basic parameters determining the photoreaction rate [116].

Porous materials were also used as active supports for catalysts and photocatalysts. Tetrahedrally coordinated metal oxide (titanium, vanadium, chromium, and molybdenum oxides) moieties can be implanted and isolated in the silica matrices of microporous zeolite and mesoporous silica materials, referred to as "single-site photocatalysts". The single-site titanium oxide photocatalyst demonstrates a high reactivity and selectivity under UV-light irradiation, while the single-site chromium oxide operates as a visible-light sensitive photocatalyst [117]. The photocatalytic H_2 production by nanosized CdS was enhanced by immobilization of CdS on porous supports, such as aluminum-substituted mesoporous silica molecular sieve (Al-HMS) [118], microporous and mesoporous silicas [119], porous polyethylene terephthalate fibers (PET) [120], and ETS-4 zeolite [121].

4.4 Spatial Control of the Reaction Environment

Judicious control of the reaction environment, which includes tailoring the transport of reactants and products to and away from the reaction sites, respectively, and confining the reaction to nanoscale volumes, is an interesting option to fine-tune the kinetics of photolytic water splitting. It allows one to address issues related to the fast back-reaction of hydrogen and oxygen, photocorrosion and reaction selectivity.

4.4.1 Tailored Transport of Reactants and Products

Experience shows that noble metal co-catalysts, which are oftentimes used to assist water reduction, at the same time tend to act as good catalysts for water formation, i.e., the unwanted back-reaction of hydrogen and oxygen to water. While this is not an issue in photoelectrochemical water splitting due to hydrogen

Fig. 19 Schematic illustrating the function of noble-metal/Cr_2O_3 core/shell nanoparticles as a co-catalyst for photocatalytic water splitting. Selective permeability of the chromia layer enables proton reduction and hydrogen evolution, while the back-reaction of hydrogen and oxygen to water is blocked. Reprinted with permission from [123]. Copyright 2009 American Chemical Society
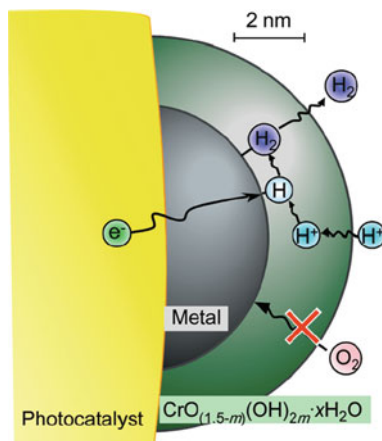
and oxygen being evolved in separate compartments, it constitutes a major limiting factor for photocatalytic water splitting, where the two species are evolved in close proximity to one another. To alleviate this problem, Domen and co-workers pioneered a concept, where the transport of reactants to the co-catalyst sites is controlled judiciously by coating the noble metal co-catalyst nanoparticles with a very thin chromium oxide shell using a photodeposition method [122]. An oxynitride photocatalyst loaded with such core/shell co-catalyst nanoparticles showed a much higher water-splitting activity than the same photocatalyst with unmodified noble-metal co-catalyst nanoparticles. Recently, extensive work by the same group [123] demonstrated that the beneficial effect of the chromia shell is related to its relative permeability for protons, hydrogen and oxygen; while the Cr_2O_3 layer is permeable to protons and evolved hydrogen molecules and does not interfere with proton reduction and hydrogen evolution, it prevents oxygen from accessing the underlying noble-metal core and therefore blocks the back reaction (Fig. 19).

This modification method has also been shown to work in combination with an oxygen evolution co-catalyst on the same photocatalyst; the addition of a Mn_3O_4 oxygen evolution co-catalyst to a Rh/Cr_2O_3 core/shell loaded GaN:ZnO photocatalyst resulted roughly in a doubling of hydrogen and oxygen evolution rates [124].

Finally, we note that the approach of blocking the back reaction via the construction of core–shell nanoarchitectures is versatile and has been applied to different semiconductors and using other shell chemistries, such as SiO_2 [125].

Kale et al. [126] reported a strategy to protect CdS quantum dots from photocorrosion by carefully controlling the interaction between reactant and photocatalyst; by partially embedding the otherwise un-photostable CdS QDs in a glass matrix, photocatalytic decomposition of H_2S to hydrogen was possible with high activity over extended time periods, thus demonstrating an increase in photostability without compromising the catalytic function.

### 4.4.2 Nanoreactors to Confine the Reaction Volume

Traditionally, catalytic systems are described in terms of interactions between the reacting species and the (open) catalytic surface. Architectures in which the interaction between the catalyst and the reactant(s) is confined to nano-liter volumes, i.e., nanoreactors, have recently attracted a great deal of attention. Various methods of confining the reaction volume have been identified and include diverse porous inorganic structures (mesoporous materials, zeolites, etc.), approaches based on molecular self-assembly (oil-in-water emulsions, liquid foams, polyelectrolyte capsules [127], co-polymer vesicles [128], lipid vesicles [129] and lipid nanotube-vesicle networks [130], etc.,) and lithographically-defined nanocavities [131].

While the most evident way in which confinement can affect a reactive system is to alter the thermodynamic properties, there are a number of other effects that can influence chemical reactions in nanospace, such as geometrical constraints in pores with a size comparable to the molecular sizes, selective adsorption of reacting molecules, and changes to the potential energy surface.

A nanoreactor may stabilize a transition state of a chemical reaction and thereby change the activation parameters of the reaction. Both enthalpic stabilization, i.e., non-covalent interactions between the transition state and the surrounding, and entropic stabilization must be considered. The latter contribution may be appreciable since the translational and rotational degrees of freedom of reactants are reduced inside a confined nanospace, leading to a pre-organization of reactants toward the transition state. Even in cases where the nanoreactor does not change the activation parameters, the kinetics of the reaction may be modified due to a locally increased concentration of reactants. This mechanism is important for low (bulk) reactant concentrations.

Stabilization of reaction intermediates, or reaction products for that matter, has the added benefit of providing new pieces of information regarding the reaction mechanism, which would not have been accessible otherwise owing to the reactive and/or labile nature of the intermediates and products; encapsulation traps intermediates and/or final products for spectroscopic analysis. Such confinement also means that several successive reactive events can be induced in a very small confined space of molecular dimensions. For example, a first photon can generate an electron that causes one bond to break and thereby creates some reaction intermediates that are trapped at the interface. A second photon can then later generate another electron that induces a second type of reactive event where the intermediates from the first event participate, and so on. This creates significant probabilities for reaction paths and products that would be vanishingly small if the reactants and intermediates were not confined. We would like to point out that this reaction mechanism, as presented, is a batch process. In order to continue, it is necessary to take the products out and to regenerate the active sites to make this a true catalytic process. There are several possible ways to achieve this, such as photo-excitation, or further reaction with other molecules. If such a process could

Fig. 20 Schematic
illustrating the mechanism of
photodissociation of water on
potassium-functionalized
graphite. Reprinted from
[144]
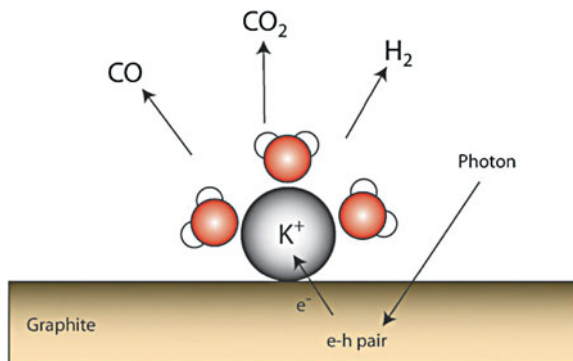
be found, the system would thereafter work as a molecular energy conversion
cycle: a true nanoscale chemical reactor.

The combined result of these effects is that confinement may increase the
activity and/or selectivity of a photocatalytic reaction. Additionally, the large
surface-area-to-volume ratio, associated with small dimensions and small
volumes, short material transport and high attempt frequency for the reaction in
nanoreactors make it possible to conduct unique processes not possible for
ordinary heterogeneous schemes [132–135].

While the nanoreactor concept has been applied to a diversity of chemical
(photo) processes [136–139], it has not yet found widespread attention in the
photocatalytic water-splitting community. Early experimental efforts report
successful incorporation of photocatalyst nanoparticles into the cavities of lipid
and surfactant vesicles and the ability of these to generate hydrogen under visible-
light illumination. The focus of these studies was, however, mainly on electron
relays for charge separation across the membrane rather than confinement effects
[140–143]. Some more recent and encouraging results for photocatalytic conver-
sion in porous media are presented in Sect. 4.3.4 above.

A recent example from our own research [144] further illustrates the
applicability of the nanoreactor concept to photocatalytic water splitting. Our
experimental system consists of a graphite substrate onto which water and
potassium are co-adsorbed. Upon photoexcitation of the graphite substrate, ener-
getic charge carriers are generated and drive photo-dissociation reactions of water
molecules at the graphite/K^+/water interface, leading to the formation of H_2, CO
and CO_2 (Fig. 20). Covering the graphite substrate with ice layers of varying
thickness and with different morphologies drastically changes the product com-
position due to (partial) confinement effects imposed by the ice layer, the product
permeability of which depends on thickness and morphology.

Although the limited body of results generated to date is perhaps mainly of
academic interest, we believe that further research efforts will demonstrate the
usefulness of the concept for large-scale industrial schemes.

4.5 Fabrication of Supported Model Systems

Enormous progress in the area of nanoscience and nanotechnology has resulted in a plethora of nanofabrication and characterization methods becoming available today. While the nano-architectures in most of the examples given in the previous sections were realized via bottom-up (often wet-chemical) approaches, the role of lithographic, top-down methods will be discussed in this section. Lithographic nanofabrication schemes such as electron beam lithography, nanosphere lithography [145] and (hole-mask) colloidal lithography [146] allow one to manufacture photocatalysts and photoelectrodes with an extremely high degree of control over structural parameters such as the size, shape and mutual arrangement of nano-structures. Given the high cost, limited speed and restrictions regarding the maximum area that can be patterned typically associated with lithographic nanofabrication approaches, we note that these methods are perhaps not expected to be of great importance for large-scale applications. They are, however, an ideal playground to fabricate supported model systems, the nano-architecture of which can be controlled and tuned accurately and over a large parameter space. By systematically varying certain key parameters, such model systems allow one to construct structure–activity maps, providing a detailed understanding of the physical and chemical processes underlying water splitting, and predictions for improved photocatalyst architectures may also be derived. An additional attractive feature of lithographically fabricated, well-defined model systems is that they are easily modeled, which is often not so for wet-chemically synthesized systems.

The concept of supported model systems has entered several fields related to energy and environment, including catalysis [147], solar cells [75], hydrogen storage materials [148] and fuel cells [149–151]. It has, to our surprise, not seen a breakthrough in the photolytic water-splitting area however. Considering the enormous, demonstrated power of this approach, we believe that it is only a matter of time until suitable model systems will be utilized to study the intriguing details of photolytic water splitting.

5 Conclusions and Outlook

There is no doubt that the world energy consumption will continue to increase rapidly, and man-made global warming is a fact, which is closely associated with our current, fossil fuel-based energy system. In order to avoid serious political unrest, energy shortages and catastrophic climate change, mankind must tap into renewable, CO_2-neutral energy sources as soon as possible. Hydrogen might be part of the answer to this immense challenge. Yet, for hydrogen to become a viable option numerous fundamental problems associated with both the production, the storage, the distribution and the use of hydrogen must still be solved. Without cost-competitive production schemes, which neither emit greenhouse gases nor have

any other negative environmental impacts, the production of hydrogen will be the bottleneck of a future hydrogen economy.

Currently, commercially available hydrogen production methods are limited to fossil fuel-based procedures and electrolysis (as driven by a variety of electricity sources). Initial efforts in the transition to the hydrogen economy may be based on these methods, with improved efficiency, lower costs and minimized carbon dioxide footprint being important prerequisites. On a longer time scale, only hydrogen which is derived from carbon-neutral sources and produced using renewable energy sources fulfills all demands posed on a sustainable energy carrier. Research and development in all fields of hydrogen production conforming to these basic criteria should be intensified, so that a wide variety of processes will become available and constitute a flexible energy system, which can be adapted to varying local conditions and requirements.

Among the renewable energy sources, we believe that solar energy will be the dominant resource for hydrogen production. Of the various pathways to harvest solar energy and use it to produce hydrogen, photolytic schemes seem to be particularly interesting, owing to their potential to achieve an attractive trade-off between high efficiency and low costs. Considering that "traditional" metal oxides, such as TiO_2, WO_3 and Fe_2O_3, have, despite several decades of investigation, not reached the target of 10% solar-to-hydrogen conversion efficiency, it is clear that further research into materials that are inexpensive, durable, abundant and environmentally-benign is needed; materials with good absorption and carrier-transport properties need to be developed, and novel interfaces need to be designed with energetic and kinetic properties favoring the water-splitting reactions while inhibiting corrosion reactions. In the case of PEC hydrogen production, the materials challenge is not only limited to the photoactive material, but also concerns the materials found in the transparent conductive layer used for charge collection. Experimental efforts in the area will be complemented by computational catalysis.

Further down the road, we foresee a significant engineering challenge to integrate improved materials and interfaces into integrated devices that can be manufactured on a commercial and large-scale basis at low cost.

But what is the role of Nanoscience and Nanotechnology (N&N) in this process? We believe that N&N will have several roles to play and that they will continue to push the field forward. Many of the improvements we have seen over the years have, in fact, been made possible thanks to N&N, albeit with a lack of consciousness and direction. This has changed over time, however, due to analytical tools to analyze very small structures becoming widely available as a consequence of developments in N&N. Today N&N are being used to systematically investigate and improve water-splitting schemes. The design of nano-composites, which feature a genuine combination of light-harvesting and charge-separation units, is perhaps the most prominent research topic at present.

Considering the rapidly growing number of important N&N contributions to other related fields, there seems to be an immense backlog demand for such schemes to be implemented in the area of photolysis. In particular, light-harvesting

and light-management schemes, which have been investigated in conjunction with solar photovoltaics, are expected to make their way into the water-splitting community in the near future. On a somewhat longer term, we expect nanoreactor concepts to gain momentum and become an area of intense research. Throughout this development, N&N will enable scientists to achieve a better understanding of the basic physics and chemistry involved in photolytic water splitting, owing to the ability to manufacture and characterize well-controlled model systems. Based on such an improved understanding, more efficient and durable systems can be constructed.

We conclude by noting that alternatives to the hydrogen economy are being and should be considered. One such example is the concept of the methanol economy [152], where methanol rather than hydrogen is used as an energy storage medium. The potential advantages of such a scheme include convenient and safe storage and handling options, and readily available transport and distribution infrastructure. Additionally, methanol may replace oil and gas resources to serve as a feedstock for the synthesis of hydrocarbons.

The most attractive scheme of producing methanol is via the photocatalytic conversion of carbon dioxide and water, i.e., using abundant and clean energy from the sun and offering ways to chemically recycle CO_2. This process has many similarities to photocatalytic hydrogen production as described in this chapter. The oxidation of water is in fact a prerequisite for both reactions, and there are thus obvious synergies. Many of the N&N concepts described here for water splitting are thus expected to be readily applicable also to photocatalytic CO_2 conversion.

References

1. Smalley RE (2005) Future global energy prosperity: the Terawatt challenge. MRS Bull 30:412–417
2. Mikkelsen M, Jørgensen M, Krebs FC (2010) The teraton challenge, a review of fixation and transformation of carbon dioxide. Energy Environ Sci 3:43–81
3. Linsebigler AL, Lu G, Yates JT Jr (1995) Photocatalysis on TiO_2 surfaces: principles, mechanisms, and selected results. Chem Rev 95:735–758
4. Maeda K, Domen K (2007) New non-oxide photocatalysts designed for overall water splitting under visible light. J Phys Chem C 111:7851–7861
5. Kudo A, Miseki Y (2009) Heterogeneous photocatalyst materials for water splitting. Chem Soc Rev 38:253–278
6. Fujishima A, Honda K (1972) Electrochemical photolysis of water at a semiconductor electrode. Nature 238:37–38
7. Carp O, Huisman CL, Reller A (2007) Photoinduced reactivity of titanium dioxide. Prog Solid State Chem 32:33–177

8. Salazar K, Kimball SM (2009) Mineral commodities summaries 2009, US Geological Survey. http://minerals.usgs.gov. Accessed 31 Aug 2010

9. Zhu J, Zhang J, Chen F et al (2005) High photocatalytic activity TiO_2 prepared by a modified sol-gel method: characterization and their photocatalytic activity for degradation of XRG and X-GL. Top Catal 35:261–268

10. Zhu J, Zhang J, Chen F et al (2005) Preparation of high photocatalytic activity TiO_2 with a bicrystalline phase containing anatase and TiO_2 (B). Mater Lett 59:3378–3381

11. Zhang HZ, Banfield JF (2000) Understanding polymorphic phase transformation behavior during growth of nanocrystalline aggregates: insights from TiO_2. J Phys Chem B 104:3481–3487

12. Chen X, Mao SS (2007) Titanium dioxide nanomaterials: synthesis, properties, modifications, and applications. Chem Rev 107:2891–2959

13. Hernández-Alonso MD, Fresno F, Suárez S et al (2009) Development of alternative photocatalysts to TiO_2: challenges and opportunities. Energy Environ Sci 2:1231–1257

14. Boschloo G, Edvinsson T, Hagfeldt A (2006) Dye-sensitized nanostructured ZnO electrodes for solar cell application. In: Tetsuo S (ed) Nanostructured materials for solar energy conversion. Elsevier, Amsterdam

15. Özgür Ü, Alivov YI, Liu C et al (2005) A comprehensive review of ZnO materials and devices. J Appl Phys 98:041301

16. Zhang H, Chen G, Bahnemann DW (2009) Photoelectrocatalytic materials for environmental applications. J Mater Chem 19:5089–5121

17. Anpo M, Chapter 10, pp 175–185; Inoue Y, Chapter 15, pp 249–261 (2002) In: Kaneko M, Okura I (eds) Photocatalysis: science and technology, Springer, New York

18. Domen K, Chapter 16, pp 261–278 (2002) In: Kaneko M, Okura I (eds) Photocatalysis: science and technology, Springer, New York

19. Rajeshwar K (2008) Hydrogen generation from irradiated semiconductor-liquid interfaces. In: Rajeshwar K, McConnell R, Licht S (eds) Solar hydrogen generation. Springer, New York

20. Kim HG, Hwang DW, Kim J et al (1999) Highly donor-doped (110) layered perovskite materials as novel photocatalysts for overall water splitting. Chem Commun 1999:1077–1078

21. Ishikawa A, Takata T, Kondo JN et al (2002) Oxysulfide $Sm_2Ti_2S_2O_5$ as a stable photocatalyst for water oxidation and reduction under visible light irradiation ($\lambda \leq 650$ nm). J Am Chem Soc 124:13547–13553

22. Kato H, Kudo A (2001) Water splitting into H_2 and O_2 on alkali tantalate photocatalysts $ATaO_3$ (A = Li, Na, and K). J Phys Chem B 105:4285–4292

23. Shangguan WF (2007) Hydrogen evolution from water splitting on nanocomposite photocatalysts. Sci Tech Adv Mater 8:76–81

24. Tian MK, Shangguan WF, Yuan J et al (2007) Promotion effect of nanosized Pt, RuO_2 and NiO_x loading on visible light-driven photocatalysts $K_4Ce_2M_{10}O_{30}$ (M = Ta, Nb) for hydrogen evolution from water decomposition. Sci Tech Adv Mater 8:82–88

25. Osterloh FE (2008) Inorganic materials as catalysts for photochemical splitting of water. Chem Mater 20:35–54

26. Asahi R, Morikawa T, Ohwaki T et al (2001) Visible-light photocatalysis in nitrogen-doped titanium oxides. Science 293:269–271

27. Hitoki G, Ishikawa A, Takata T et al (2002) Ta_3N_5 as a novel visible light-driven photocatalyst ($\lambda < 600$ nm). Chem Lett 33:736–737

28. Sato J, Saito N, Yamada Y et al (2005) RuO_2-loaded β-Ge_3N_4 as a non-oxide photocatalyst for overall water splitting. J Am Chem Soc 127:4150–4151

29. Kida T, Minami Y, Guan G et al (2006) Photocatalytic activity of gallium nitride for producing hydrogen from water under light irradiation. J Mater Sci 41:3527–3534

30. Hara M, Takata T, Kondo JN et al (2004) Photocatalytic reduction of water by TaON under visible light irradiation. Catal Today 90:313–317

31. Yamasita D, Takata T, Hara M et al (2004) Recent progress of visible-light-driven heterogeneous photocatalysts for overall water splitting. Solid State Ionics 172:591–595
32. Kasahara A, Nukumizu K, Takata T et al (2003) LaTiO$_2$N as a visible-light ($\leq$600 nm)-driven photocatalyst (2). J Phys Chem B 107:791–797
33. Liu M, You W, Lei Z et al. (2004) Water reduction and oxidation on Pt–Ru/Y$_2$Ta$_2$O$_5$N$_2$ catalyst under visible light irradiation. Chem Commun 2004: 2192–2193
34. Maeda K, Teramura K, Lu DL et al (2006) Photocatalyst releasing hydrogen from water-enhancing catalytic performance holds promise for hydrogen production by water splitting in sunlight. Nature 440:295
35. Lee Y, Terashima H, Shimodaira Y et al (2007) Zinc germanium oxynitride as a photocatalyst for overall water splitting under visible light. J Phys Chem C 111:1042–1048
36. Ishikawa A, Takata T, Matsumura T et al (2004) Oxysulfides Ln$_2$Ti$_2$S$_2$O$_5$ as stable photocatalysts for water oxidation and reduction under visible-light irradiation. J Phys Chem B 108:2637–2642
37. Finklea HO (1988) Semiconductor electrodes. Elsevier, Amsterdam
38. Heller A (1984) Hydrogen-evolving solar cells. Science 223:1141–1148
39. Khaselev O, Turner JA (1998) A monolithic photovoltaic-photoelectrochemical device for hydrogen production via water splitting. Science 280:425–427
40. Taniguchi Y, Yoneyama H, Tamura H (1983) Hydrogen evolution on surface-modified silicon powder photocatalysts in aqueous ethanol solutions. Chem Lett 12:269–272
41. Yoneyama H, Matsumoto N, Tamura H (1986) Photocatalytic decomposition of formic acid on platinized n-type silicon powder in aqueous solution. Bull Chem Soc Jpn 59:3302–3304
42. Sakai Y, Sugahara S, Matsumura M et al (1988) Photoelectrochemical water splitting by tandem type and heterojunction amorphous silicon electrodes. Can J Chem 66:1853–1856
43. Frame FA, Carroll EC, Larsen DS et al (2008) First demonstration of CdSe as a photocatalyst for hydrogen evolution from water under UV and visible light. Chem Commun 19:2206–2208
44. Schürch D, Currao A, Sarkar S et al (2002) The silver chloride photoanode in photoelectrochemical water splitting. J Phys Chem B 106:12764–12775
45. Currao A, Reddy VR, van Veen MK et al (2004) Water splitting with silver chloride photoanodes and amorphous silicon solar cells. Photochem Photobiol Sci 3:1017–1025
46. Gao Y, Wang Y, Wang Y (2007) Photocatalytic hydrogen evolution from water on SiC under visible light irradiation. React Kinet Catal Lett 91:13–19
47. Levy B (1997) Photochemistry of nanostructured materials for energy applications. J Electroceramics 1:239–272
48. Stroyuk AL, Kryukov AI, Kuchmii SY et al (2009) Semiconductor photocatalytic systems for the production of hydrogen by the action of visible light. Theor Exp Chem 45: 209–233
49. Li D, Haneda H, Hishita S et al (2005) Fluorine-doped TiO$_2$ powders prepared by spray pyrolysis and their improved photocatalytic activity for decomposition of gas-phase acetaldehyde. J Fluor Chem 126:69–77
50. Lin ZS, Orlov A, Lambert RM et al (2005) New insights into the origin of visible light photocatalytic activity of nitrogen-doped and oxygen-deficient anatase TiO$_2$. J Phys Chem B 109:20948–20952
51. Nakamura R, Tanaka T, Nakato Y (2004) Mechanism for visible light responses in anodic photocurrents at n-doped TiO$_2$ film electrodes. J Phys Chem B 108:10617–10620
52. Kamat PV (2007) Meeting the clean energy demand: nanostructure architectures for solar energy conversion. J Phys Chem C 111:2834–2860
53. Baba R, Nakabayashi S, Fujishima A et al (1985) Investigation of the mechanism of hydrogen evolution during photocatalytic water decomposition on metal-loaded semiconductor powders. J Phys Chem 89:1902–1905
54. Nosaka Y, Norimatsu K, Miyama H (1984) The function of metals in metal-compounded semiconductor photocatalysts. Chem Phys Lett 106:128–131

55. Subramanian V, Wolf EE, Kamat PV (2004) Catalysis with TiO_2/Au nanocomposites effect of metal particle size on the Fermi level equilibration. J Am Chem Soc 126:4943–4950

56. Sayama K, Mukasa K, Abe R et al (2002) A new photocatalytic water splitting system under visible light irradiation mimicking a Z-scheme mechanism in photosynthesis. J Photochem Photobio A: Chem 148:71–77

57. Tada H, Mitsui T, Kiyonaga T et al (2006) All-solid-state Z-scheme in CdS–Au–TiO_2 three-component nanojunction system. Nature Mater 5:782–786

58. Campbell P, Green MA (1987) Light trapping properties of pyramidally textured surfaces. J Appl Phys 62:243–249

59. Heine C, Morf RH (1995) Submicrometer gratings for solar energy applications. Appl Optics 34:2476–2482

60. Ito S, Murakami TN, Comte P et al (2008) Fabrication of thin film dye sensitized solar cells with solar to electric power conversion efficiency over 10%. Thin Solid Films 516:4613–4619

61. Vahala KJ (2003) Optical microcavities. Nature 424:839–846

62. Halaoui LI, Abrams NM, Mallouk TE (2005) Increasing the conversion efficiency of dye-sensitized TiO_2 photoelectrochemical cells by coupling to photonic crystals. J Phys Chem B 109:6334–6342

63. Bermel P, Luo C, Zeng L et al (2007) Improving thin-film crystalline silicon solar cell efficiencies with photonic crystals. Opt Express 15:16986–17000

64. Wiersma DS, Sapienza R, Mujumdar S et al (2005) Optics of nanostructured dielectrics. J Opt A: Pure Appl Opt 7:S190–S197

65. Mayer B, Madronich S (2004) Actinic flux and photolysis in water droplets: Mie calculations and geometrical optics limit. Atmos Chem Phys 4:2241–2250

66. Robinson JT, Manolatou C, Chen L et al (2005) Ultrasmall mode volumes in dielectric optical microcavities. Phys Rev Lett 95:143901

67. Kreibig U, Vollmer M (1995) Optical properties of metal clusters. Springer, Berlin

68. Coyle S, Netti MC, Baumberg JJ et al (2001) Confined plasmons in metallic nanocavities. Phys Rev Lett 87:176801

69. Atwater HA, Polman A (2010) Plasmonics for improved photovoltaic devices. Nat Mater 9:205–213

70. Tsai F-J, Wang J-Y, Huang J-J et al (2010) Absorption enhancement of an amorphous Si solar cell through surface plasmon-induced scattering with metal nanoparticles. Opt Express 18:A207–A220

71. Hägglund C, Zäch M, Petersson G et al (2008) Electromagnetic coupling of light into a silicon solar cell by nanodisk plasmons. Appl Phys Lett 92:053110

72. Ferry VE, Sweatlock LA, Pacifici D et al (2008) Plasmonic nanostructure design for efficient light coupling into solar cells. Nano Lett 8:4391–4397

73. Bai W, Gan Q, Bartoli F et al (2009) Design of plasmonic back structures for efficiency enhancement of thin-film amorphous Si solar cells. Optics Lett 34:3725–3727

74. Kirkengen M, Bergli J, Galperin YM (2007) Direct generation of charge carriers in c-Si solar cells due to embedded nanoparticles. J Appl Phys 102:093713

75. Hägglund C, Zäch M, Kasemo B (2008) Enhanced charge carrier generation in dye sensitized solar cells by nanoparticle plasmons. Appl Phys Lett 92:013113

76. Kelzenberg MD, Boettcher SW, Petykiewicz JA et al (2010) Enhanced absorption and carrier collection in Si wire arrays for photovoltaic applications. Nat Mater 9:239–244

77. Zhu J, Hsu C-M, Yu Z et al (2010) Nanodome solar cells with efficient light management and self-cleaning. Nano Lett 10:1979–1984

78. Brus L (2008) Noble metal nanocrystals: plasmon electron transfer photochemistry and single-molecule Raman spectroscopy. Acc Chem Res 41:1742–1749

79. Watanabe K, Menzel D, Nilius N et al (2006) Photochemistry on metal nanoparticles. Chem Rev 106:4301–4320

80. Awazu K, Fujimaki M, Rockstuhl C et al (2008) A plasmonic photocatalyst consisting of silver nanoparticles embedded in titanium dioxide. J Am Chem Soc 130:1676–1680

81. Christopher P, Ingram DB, Linic S (2010) Enhancing photochemical activity of semiconductor nanoparticles with optically active Ag nanostructures: photochemistry mediated by Ag surface plasmons. J Phys Chem C 114:9173–9177

82. Tian Y, Tatsuma T (2005) Mechanisms and applications of plasmon-induced charge separation at TiO_2 films loaded with gold nanoparticles. J Am Chem Soc 127:7632–7637

83. Ertl G, Knözinger H, Weitkamp J (1997) Handbook of heterogeneous catalysis. Wiley, Weinheim

84. Haruta M, Kobayashi T, Sano H et al (1987) Novel gold catalysts for the oxidation of carbon-monoxide at a temperature far below 0°C. Chem Lett 2:405–406

85. Maira AJ, Yeung KL, Lee CY et al (2000) Size effects in gas-phase photo-oxidation of trichloroethylene using nanometer-sized TiO_2 catalysts. J Catal 192:185–196

86. Suzuki Y, Ngamsinlapasathian S, Yoshida R et al (2006) Partially nanowire-structured TiO_2 electrode for dye-sensitized solar cells. Cent Eur J Chem 4:476–488

87. Beermann N, Vayssieres L, Lindquist S-E et al (2000) Photoelectrochemical studies of oriented nanorod thin films of hematite. J Electrochem Soc 147:2456–2461

88. van de Krol R, Liang Y, Schoonman J (2008) Solar hydrogen production with nanostructured metal oxides. J Mater Chem 2008(18):2311–2320

89. Kay A, Cesar I, Grätzel M (2006) New benchmark for water photooxidation by nanostructured α-Fe_2O_3 films. J. Am. Chem Soc 128:15714–15721

90. Lindgren T, Wang H, Beermann N et al (2002) Aqueous photoelectrochemistry of hematite nanorod array. Sol Energy Mater Sol Cells 71:231–243

91. Wang Y, Zhang Z, Zhu Y et al (2008) Nanostructured VO_2 photocatalysts for hydrogen production. ACS Nano 2:1492–1496

92. Feng X, LaTempa TJ, Basham JI et al (2010) Ta_3N_5 nanotube arrays for visible light water photoelectrolysis. Nano Lett 10:948–952

93. Shankar K, Basham JI, Allam NK et al (2009) Recent advances in the use of TiO_2 nanotube and nanowire arrays for oxidative photoelectrochemistry. J Phys Chem C 113:6327–6359

94. Khan SUM, Sultana T (2003) Photoresponse of n-TiO_2 thin film and nanowire electrodes. Sol Energy Mater Sol Cells 76:211–221

95. Wolcott A, Smith WA, Kuykendall TR et al (2009) Photoelectrochemical water splitting using dense and aligned TiO_2 nanorod arrays. Small 5:104–111

96. Mor GK, Shankar K, Paulose M et al (2005) Enhanced photocleavage of water using titania nanotube arrays. Nano Lett 5:191–195

97. Lin CH, Lee CH, Chao JH et al (2004) Photocatalytic generation of H_2 gas from neat ethanol over Pt/TiO_2 nanotube catalysts. Catal Lett 98:61–66

98. Nam W, Han GY (2007) Preparation and characterization of anodized Pt-TiO_2 nanotube arrays for water splitting. J Chem Eng Jpn 40:266–269

99. Khan MA, Akhtar MS, Woo SI et al (2008) Enhanced photoresponse under visible light in Pt ionized TiO_2 nanotube for the photocatalytic splitting of water. Catal Commun 10:1–5

100. Thimsen E, Rastgar N, Biswas P (2008) Nanostructured TiO_2 films with controlled morphology synthesized in a single step process: performance of dye-sensitized solar cells and photo water splitting. J Phys Chem C 112:4134–4140

101. Jitputti J, Suzuki Y, Yoshikawa S (2008) Synthesis of TiO_2 nanowires and their photocatalytic activity for hydrogen evolution. Catal Commun 9:1265–1271

102. Kuo HL, Kuo CY, Liu CH et al (2007) A highly active bi-crystalline photocatalyst consisting of TiO_2 (B) nanotube and anatase particle for producing H_2 gas from neat ethanol. Catal Lett 113:7–12

103. Lin CH, Chao JH, Liu CH et al (2008) Effect of calcination temperature on the structure of a Pt/TiO_2 (B) nanofiber and its photocatalytic activity in generating H_2. Langmuir 24:9907–9915

104. Janet CM, Viswanath RP (2006) Large scale synthesis of CdS nanorods and its utilization in photo-catalytic H_2 production. Nanotechnology 17:5271–5277

105. Jang JS, Joshi UA, Lee JS (2007) Solvothermal synthesis of CdS nanowires for photocatalytic hydrogen and electricity production. J. Phys Chem C 111:13280–13287

106. Wang G, Yang X, Qian F et al (2010) Double-sided CdS and CdSe quantum dots co-sensitized ZnO nanowire arrays for photoelectrochemical hydrogen generation. Nano Lett 10:1088–1092
107. Costi R, Saunders AE, Elmalem E et al (2008) Visible light-induced charge retention and photocatalysis with hybrid CdSe-Au nanodumbbells. Nano Lett 8:637–641
108. Amirav L, Alivisatos AP (2010) Photocatalytic hydrogen production with tunable nanorod heterostructures. J Phys Chem Lett 1:1051–1054
109. Qu Y, Liao L, Cheng R et al (2010) Rational design and synthesis of freestanding photoelectric nanodevices as highly efficient photocatalysts. Nano Lett 10:1941–1949
110. Yu JG, Qi LF, Jaroniec M (2010) Hydrogen Production by Photocatalytic Water Splitting over Pt/TiO_2 nanosheets with exposed (001) facets. J Phys Chem C 114:13118–13125
111. Liu G, Yang HG, Wang XW et al (2009) Visible light responsive nitrogen doped anatase TiO_2 sheets with dominant 001 facets derived from TiN. J Am Chem Soc 131:12868–12869
112. Liu G, Yang HG, Wang XW et al (2009) Enhanced photoactivity of oxygen-deficient anatase TiO_2 sheets with dominant 001 facets. J Phys Chem C 113:21784–21788
113. Youngblood WJ, Lee SHA, Maeda K et al (2009) Visible light water splitting using dye-sensitized oxide semiconductors. Acc Chem Res 42:1966–1973
114. Yi H, Peng T, Ke D et al (2008) Photocatalytic H_2 production from methanol aqueous solution over titania nanoparticles with mesostructures. Int J Hydrogen Energy 33:672–678
115. Lakshminarasimhan N, Bae E, Choi W (2007) Enhanced photocatalytic production of H_2 on mesoporous TiO_2 prepared by template-free method: role of interparticle charge transfer. J Phys Chem C 111:15244–15250
116. Korzhak A, Ermokhina N, Stroyuk A et al (2008) Photocatalytic hydrogen evolution over mesoporous TiO_2/metal nanocomposites. J Photochem Photobio A: Chem 198:126–134
117. Yamashita H, Mori K (2007) Applications of single-site photocatalysts implanted within the silica matrixes of zeolite and mesoporous silica. Chem Lett 36:348–353
118. Zhang YJ, Zhang L (2008) Synthesis of composite material CdS/Al-HMS and hydrogen production by photocatalytic pollutant degradation under visible light irradiation. J Inorg Mater 23:66–70
119. Ryu SY, Balcerski W, Lee TK et al (2007) Photocatalytic production of hydrogen from water with visible light using hybrid catalysts of CdS attached to microporous and mesoporous silicas. J Phys Chem C 111:18195–18203
120. Lunawat PS, Senapati S, Kumar R et al (2007) Visible light-induced splitting of water using CdS nanocrystallites immobilized over water-repellant polymeric surface Int. J Hydrogen Energy 32:2784–2790
121. Guan GQ, Kida T, Kusakabe K et al (2004) Photocatalytic H_2 evolution under visible light irradiation on CdS/ETS-4 composite. Chem Phys Lett 385:319–322
122. Maeda K, Teramura K, Lu D et al (2006) Noble-metal/Cr_2O_3 core/shell nanoparticles as a co-catalyst for photocatalytic overall water splitting. Angew Chem Int Ed 45:7806–7809
123. Yoshida M, Takanabe K, Maeda K et al (2009) Role and function of noble-metal/Cr-layer core/shell structure co-catalysts for photocatalytic overall water splitting studied by model electrodes. J Phys Chem C 113:10151–10157
124. Maeda K, Xiong A, Yoshinaga T et al (2010) Photocatalytic overall water splitting promoted by two co-catalysts for hydrogen and oxygen evolution under visible light. Angew Chem Int Ed. 49:4096–4099
125. Ikeda S, Hirao K, Ishino S et al (2006) Preparation of platinized strontium titanate covered with hollow silica and its activity for overall water splitting in a novel phase-boundary photocatalytic system. Catal Today 117:343–349
126. Kale BB, Baeg J-O, Apte SK et al (2007) Confinement of nano CdS in designated glass: a novel functionality of quantum dot-glass nanosystems in solar hydrogen production. J Mater Chem 17:4297–4303

127. Dähne L, Leporatti S, Donath E et al (2001) Fabrication of micro reaction cages with tailored properties. J Am Chem Soc 123:5431–5436
128. Nardin C, Thoeni S, Widmer J et al (2000) Nanoreactors based on (polymerized) ABA-triblock copolymer vesicles. Chem Commun 2000:1433–1434
129. Ruysschaert T, Germain M, da Silva Gomes JFP et al (2004) Liposome-based nanocapsules. IEEE Trans Nanobiosci 3:49–55
130. Karlsson M, Davidson M, Karlsson R et al (2004) Biomimetic nanoscale reactors and networks. Ann Rev Phys Chem 55:613–649
131. Doshi DA, Huesing N, Lu M et al (2000) Optically defined multifunctional patterning of photosensitive thin-film silica mesophases. Science 290:107–111
132. Shtykov SN (2002) Chemical analysis in nanoreactors: main concepts and applications. J Anal Chem 57:859–868
133. Herrmann J-M (2005) Heterogeneous photocatalysis: state of the art and present applications. Top Catal 34:49–65
134. Santiso EE, George AM, Turner CH et al (2005) Adsorption and catalysis: the effect of confinement on chemical reactions. Appl Surf Sci 252:766–777
135. Shchukin DG, Sviridov DV (2006) Photocatalytic processes in spatially confined micro- and nanoreactors. J Photochem Photobiol C 7:23–39
136. Koblenz TS, Wassenaar J, Reek JNH (2008) Reactivity within a confined self-assembled nanospace. Chem Soc Rev 37:247–262
137. Li J, Zeng HC (2005) Size tuning, functionalization, and reactivation of Au in TiO_2 nanoreactors. Angew Chem Int Ed 44:4342–4345
138. Yen CW, Mahmoud MA, El-Sayed MA (2009) Photocatalysis in gold nanocage nanoreactors. J Phys Chem A 113:4340–4345
139. Harris C, Kamat PV (2009) Photocatalysis with CdSe nanoparticles in confined media: mapping charge transfer events in the subpicosecond to second timescales. ACS Nano 3:682–690
140. Parmon VN, Lymar SV, Tsvetkov IM et al (1983) Development of microheterogeneous systems based on lipid vesicles for photocatalytic charge separation in molecular converters of solar energy. J Mol Catal 21:353–363
141. Khramov MI, Parmon VN (1993) Synthesis of ultrafine particles of transition metal sulphides in the cavities of lipid vesicles and the light-stimulated transmembrane electron transfer catalysed by these particles. J Photochem Photobiol A: Chem 71:279–284
142. Efimova EV, Lymar SV, Parmon VN (1994) 1,4-bis(1, 2, 6-triphenyl-4-pyridyl)benzene as a novel hydrophobic eletron relay for dihydrogen evolution in photocatalytic systems based on lipid vesicles. J. Photochem Photobiol A: Chem 83:153–159
143. Tricot Y-M, Emeren Å, Fendler JH (1985) In situ generation of catalyst-coated CdS particles in polymerized and unpolymerized surfactant vesicles and their utilization for efficient visible-light induced hydrogen production. J Phys Chem 89:4721–4726
144. Bergeld J, Kasemo B, Chakarov D (2008) Photocatalytic reactions at the graphite/ice interface. Phys Chem Chem Phys 10:1151–1155
145. Hulteen JC, van Dyne RP (1994) Nanosphere lithography: a materials general fabrication process for periodic particle array surfaces. J Vac Sci Technol A 13:1553–1558
146. Fredriksson H, Alaverdyan Y, Dmitriev A et al (2007) Hole-mask colloidal lithography. Adv Mater 19:4297–4302
147. Johanek V, Laurin M, Grant AW et al (2004) Fluctuations and bistabilities on catalyst nanoparticles. Science 304:1639–1644
148. Langhammer C, Zoric I, Kasemo B et al (2007) Hydrogen storage in Pd nanodisks characterized with a novel nanoplasmonic sensing scheme. Nano Lett 7:3122–3127
149. Komanicky V, Iddir H, Chang KC et al (2009) Shape-dependent activity of platinum array catalyst. J Am Chem Soc 131:5732–5733

150. Brown EC, Wilke SK, Boyd DA et al (2010) Polymer sphere lithography for solid oxide fuel cells: a route to functional, well-defined electrode structures. J Mater Chem 20:2190–2196
151. Seidel YE, Scheider A, Jusys Z et al (2010) Transport effects in the electrooxidation of methanol studied on nanostructured Pt/glassy carbon electrodes. Langmuir 26:3569–3578
152. Olah GA, Goeppert A, Prakash GKS (2009) Beyond oil and gas: the methanol economy, 2nd edn. Wiley-VCH, Weinheim